ERDC/CHL TR-06-12

US Army Corps
of Engineers®
Engineer Research and
Development Center

Coastal Navigation Hydrodynamics Program

Including Nearshore Processes in Phase-Averaged Hydrodynamic Models

Bradley D. Johnson

August 2006

Coastal and Hydraulics Laboratory

Coastal Navigation Hydrodynamics Program

ERDC/CHL TR-06-12
August 2006

Including Nearshore Processes in Phase-Averaged Hydrodynamic Models

Bradley D. Johnson

Coastal and Hydraulics Laboratory
U.S. Army Engineer Research and Development Center
3909 Halls Ferry Road
Vicksburg, MS 39180-6199

Final report

Prepared for U.S. Army Corps of Engineers
Washington, DC 20314-1000

Abstract: The large spatial and time scales of the numerical modeling projects of the U.S. Army Corps of Engineers (USACE) requires the use of computationally efficient phase-averaged hydrodynamic models derived by averaging the equations of motion over a representative short wave period. Guidance in modeling nearshore regions with phase-averaged hydrodynamic models is provided herein. Physical processes unique to the surf zone are described along with methods of incorporating these effects to improve hydrodynamic predictions. Comparisons to detailed measurements from a laboratory basin experiment are used to demonstrate the significance of including processes unique to nearshore regions. To provide guidance that is applicable to varied phase-averaged models, details of the implementation are not provided herein, and the focus is on conceptual models.

Contents

Figures and Tables

Figures

Tables

Preface

The work described herein was conducted at the U.S. Army Engineer Research and Development Center (ERDC), Coastal and Hydraulics Laboratory (CHL), under the Coastal Navigation Hydrodynamics Program work unit Advanced Nearshore Circulation and Sediment Transport. Overall program management is directed by the Hydraulic Design section of Headquarters, U. S. Army Corps of Engineers (HQUSACE). Program Monitors are Charles Chesnutt, Barry Holliday, and Mike Klosterman, HQUSACE. The Program Manager is James Clausner, CHL. This study was conducted under the general supervision of Ty Wamsley, Chief, Coastal Processes Branch (CPB); Bruce Ebersole, Chief, Flood and Storm Protection Division, CHL; Dr. William D. Martin, Deputy Director, CHL: and Thomas W. Richardson, Director, CHL. The report was prepared by Dr. Bradley D. Johnson, CPB. Drs. Jane McKee Smith (CPB) and Joe Z. Gailani (CPB) provided technical review of this report.

Dr. James R. Houston was Director of ERDC. COL Richard B. Jenkins was Commander and Executive Director.

1 Introduction

This document provides guidance in modeling nearshore regions with phase-averaged hydrodynamic models where phase-averaged models are derived by averaging the equations of motion over a representative short wave period. Physical processes unique to the surf zone are described along with methods of incorporating these effects to improve hydrodynamic predictions. Comparisons to detailed measurements from a laboratory basin experiment are used to demonstrate the significance of including processes unique to nearshore regions. To provide guidance that is applicable to varied phase-averaged models, details of the implementation are not provided herein, and the focus is on conceptual models.

The coastal engineering community has witnessed a shift in focus over the past several decades from physical modeling of hydrodynamics to the use of numerical models. A suitable set of equations conserving mass, momentum, and energy do not suffer the high cost and scale effects of physical models. Numerical models, however, rely on a set of discritized and simplified equations, and nonphysical and unrealistic solutions can develop. In the narrow strip of coast defined as the nearshore region (within a few surf zone widths of the coast), the physical processes that play a prominent role in the current profiles are poorly understood and differ significantly from the dominant effects in deeper water. As a result, the nearshore region with the most intensive sediment transport is poorly described mathematically in most phase-averaged models.

The phase resolving equations of fluid motion may be best suited for a physically based prediction of sediment transport in the surf zone. Lin and Liu (1998), for example, solved the Reynolds equations with an algebraic nonlinear Reynolds stress model. Karambas and Koutitas (2002) and Kobayashi and Johnson (2001) used Boussinesq and nonlinear shallow-water formulations, respectively. These time-dependent numerical models, however, are not suitable to most practical engineering problems due to the prohibitively large computation time, and spatial domains are typically limited to several kilometers. The problem of computational cost is further exacerbated if the time-step is reduced to adequately resolve the short waves in the inner surf or to maintain stability at a moving shoreline boundary.

For engineering application, hydrodynamics in the nearshore are typically examined at two distinct time scales, with a time-averaging procedure that parameterizes the short-wave motions as a forcing function for the low-frequency or steady currents. A further reduction of complexity is realized with depth-averaging, thus eliminating the moving boundary condition of the free surface. These simplifications lead to a tractable system composed of a short-wave driver coupled to a circulation model. The prediction of coastal flooding and water levels in the nearshore has reached some level of maturity through the solution of these systems, although details such as wave nonlinearity and depth variation are not computed directly and are dependent on empirical closures. These shortcomings present a serious impediment to nearshore sediment transport prediction capability, where reliable predictions are dependent on a three-dimensional (3-D) description of the hydrodynamics. Concentrations of sediment are known to be orders of magnitude larger near the bed where fluid velocities are, in general, smaller than the depth-averaged value. Therefore, it is of practical importance to predict the vertical variation of nearshore currents.

This report focuses on practical methods for developing realistic hydrodynamic predictions without the numerical cost and complexity associated with a fully 3-D fluid flow solution and a coupled turbulence closure scheme. References for the more detailed physical processes are provided for the interested reader. The preliminary step in the eventual computation of nearshore currents is developing a two-dimensional (2-D) field of wave heights and directions, depth-averaged currents, and slowly-varying free-surface position. The prediction of wave heights has been the topic of intensive research for the past several decades, and it is assumed hereafter that accurate free-surface statistics and depth-averaged hydrodynamics are available. Guidance on computing distributions of wave heights and the associated radiation stresses is provided in Smith et al. (2001). Further, a suitable two-dimensional horizontal (2-DH) hydrodynamic solution is assumed to be available.

The following section provides a brief overview of laboratory data that will be used to illustrate the significance of various nearshore current processes. Then the momentum balance is presented and populated with laboratory data. The computed bottom shear stress is compared with models and parameterizations. Finally, two methods for developing the depth dependence of the phase-averaged current field are presented and compared with laboratory data.

2 Laboratory Measurements for Illustration

A brief description of the Large-scale Sediment Transport Facility (LSTF) used to collect nearshore processes data follows. These data are used to illustrate the spatial variation waves, currents, and forcing functions. The interested reader is referred to the detailed report on the LSTF design, instrumentation, and capabilities of the tank by Hamilton et al. (2001). In an attempt to avoid ambiguity, the wave heights and mean free surface used in the examples are not model predictions, but are based on detailed laboratory data. Likewise, when examining the contribution of current-current interaction terms, the measured currents are used to develop the most accurate assessment.

The LSTF measures approximately 25 m in the cross-shore by 30 m alongshore where the walls are angled relative to a cross-shore transect to act as wave guides and minimize interference with the propagation of obliquely incident waves (Figure 1). Unidirectional waves were generated at a depth of 0.9 m with four synchronized paddles rotated to create long crests oriented 10 deg from the long, straight shoreline. A pump system externally recirculates the wave-generated longshore current from the downstream boundary to the upstream boundary of the facility, thus allowing the laboratory basin to function as an infinitely long coast. The cross-shore distribution of the longshore current is regulated by 20 independently controlled pumps through 20 channels at the downdrift end of the tank. Determining the proper pump rate was an iterative procedure, and the procedure details are given in Hamilton and Ebersole (2001).

LSTF sand bed

The LSTF sand beach comprises well-sorted quartz sand with a median grain diameter of 0.15 mm. Before the data collection began, the beach was exposed to wave action until a stable profile was realized (Wang et al. 2002). Beach profiles were measured with a bottom-tracking profiler with a sampling rate sufficiently rapid to resolve the sand ripples. Figure 2 presents a measured profile near the center of the tank at y = 22 m and smaller scale detail plots showing the ripple geometry at three cross-shore locations. The bed stresses in a surf zone are typically large enough that ripples are washed out over a portion of the entire breaking region. Sand transport over the bar, in particular, is usually sheet flow transport.

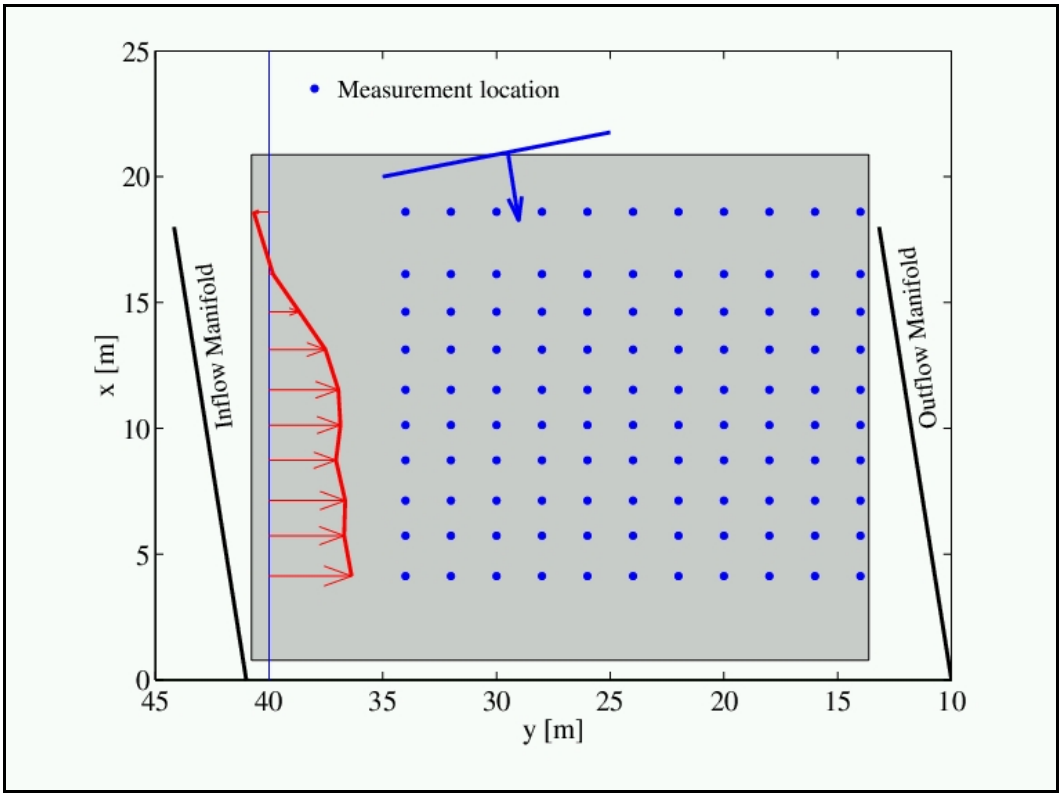

Figure 1. Plan view of LSTF where the shaded gray region shows coverage of the bathymetry measurement, and the positions of the measurement locations for the horizontal coverage are depicted (•).

However, the flow conditions of the test detailed herein were such that ripples were present over the majority of the surf zone, including the bar. It is likely that a slight increase in wave height would have produced a change in bed state (Tajima 2004). Ripples were statistically uniform along the beach, and with the exception of the swash zone, were reasonably uniform in height and length across the beach. Directly seaward of the swash zone, ripples measured approximately 1 cm in height and 8 cm in length. The height and length of ripples in the midsurf zone measured 0.7 cm and 8 cm, similar in dimension to the ripples measured in the region immediately seaward of the bar with 0.6 cm and 7 cm. In combined wave and current environments, ripple orientation can become irregular for sufficiently strong currents. In the portion of the tank that is used for this study, the ripple crests were visually observed to be wave-dominated, meaning that the crests were oriented essentially perpendicular to the wave propagation direction, from ~10 to 5 deg relative to a cross-shore transect.

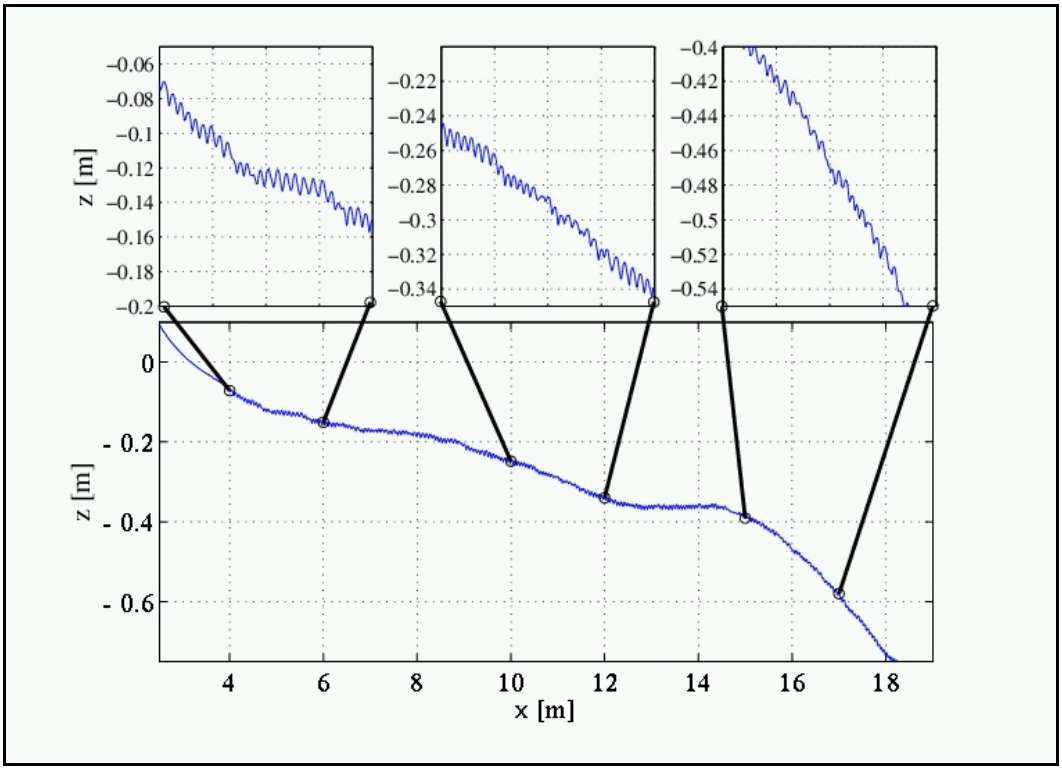

Figure 2. Bottom profile and detail of vortex ripples at y = 22 m.

LSTF data collection

Synchronized free-surface elevations and velocities were collected from a movable instrument bridge spanning a cross-shore transect. Ten capacitance-type surface piercing wave gauges, sampled at 20 Hz, were used to collect the free-surface elevation. Velocity data were collected with acoustic Doppler velocimeters (ADV) at the same cross-shore position and synchronized with the wave gauge signals. Cross-shore instrument position is given in Table 1. Each LSTF run was 10 min long, and complete horizontal and vertical coverage was accomplished by moving either the bridge or the instrument elevation. Stationarity in the wave field was assured by using the same wave paddle-position time series for each run. The data were collected in two stages. The first stage focused on broad horizontal coverage where velocity measurements were taken at one-third of the water depth from the bottom, and the horizontal measurement locations are shown in Figure 1. Detailed velocity data at 10 positions over the vertical column were compiled during the second stage of each test for a single cross-shore transect at y = 22 m. The vertical positioning of the measurement locations is shown in Figure 3.

Table 1. Cross-shore positioning of instruments.

ADV and wave gauge No.	Cross-shore position (m)
1	4.125
2	5.725
3	7.125
4	8.725
5	10.125
6	11.525
7	13.125
8	14.625
9	16.125
10	18.600

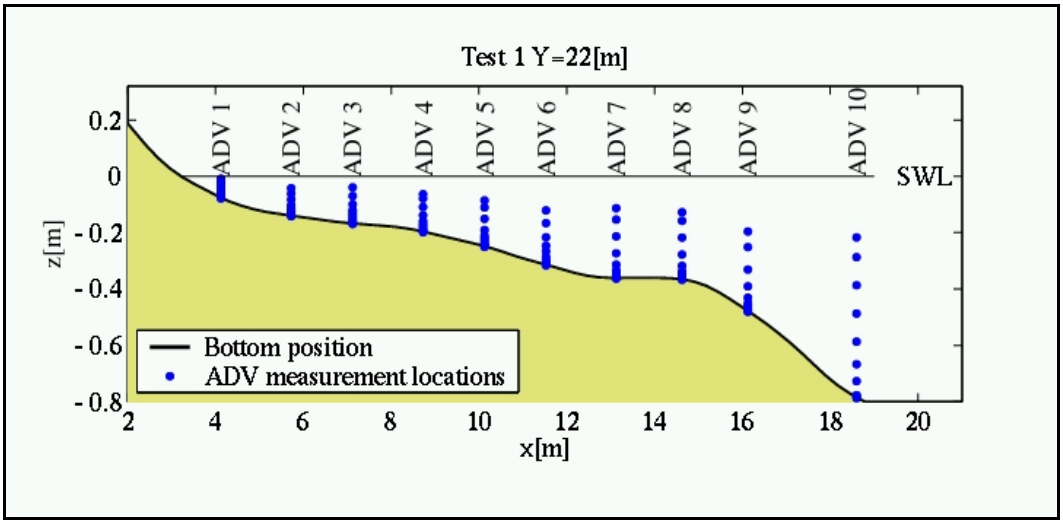

Figure 3. Measurement locations for vertical coverage phase are depicted (•).

LSTF waves

Irregular waves with TMA (Bouws *et al.* 1985) spectral shape were generated with a peak period of $T_p = 1.5$ sec and a spectral peakedness parameter $\gamma = 3.3$. A piston-type wave paddle was used to generate waves in 0.9 m of water, and the spectra of the free-surface elevation measured seaward of the breaking region at wave gauge 10 is shown in Figure 4. Based on the data at wave gauge 10, the root-mean-squared wave height is 0.185 m, where H_{rms} is the high-pass filtered (f > 0.33 Hz) root-mean-squared wave height. Spectral analysis of the variation in free-surface position indicates significant low-frequency energy in the inner surf zone that is consistent with standing waves due to resonance in the closed basin. While the tank

resonance has a pronounced effect on the free-surface variation near the shoreline, these long waves do not break and do not contribute to the radiation stress. Thus, it is argued that the most meaningful representation of wave height for this study of momentum flux excludes the low-frequency components. The wave height is computed as $H_{rms} = \sqrt{8} m_o(f > 1/3\text{s})$ where $m_o(f > 1/3\text{s})$ is the zero-moment of the variance spectrum including only frequencies larger than half of the peak frequency. The irregular waves are classified as spilling breakers with a surf similarity parameter $\xi = 0.15$ based on H_{rms}.

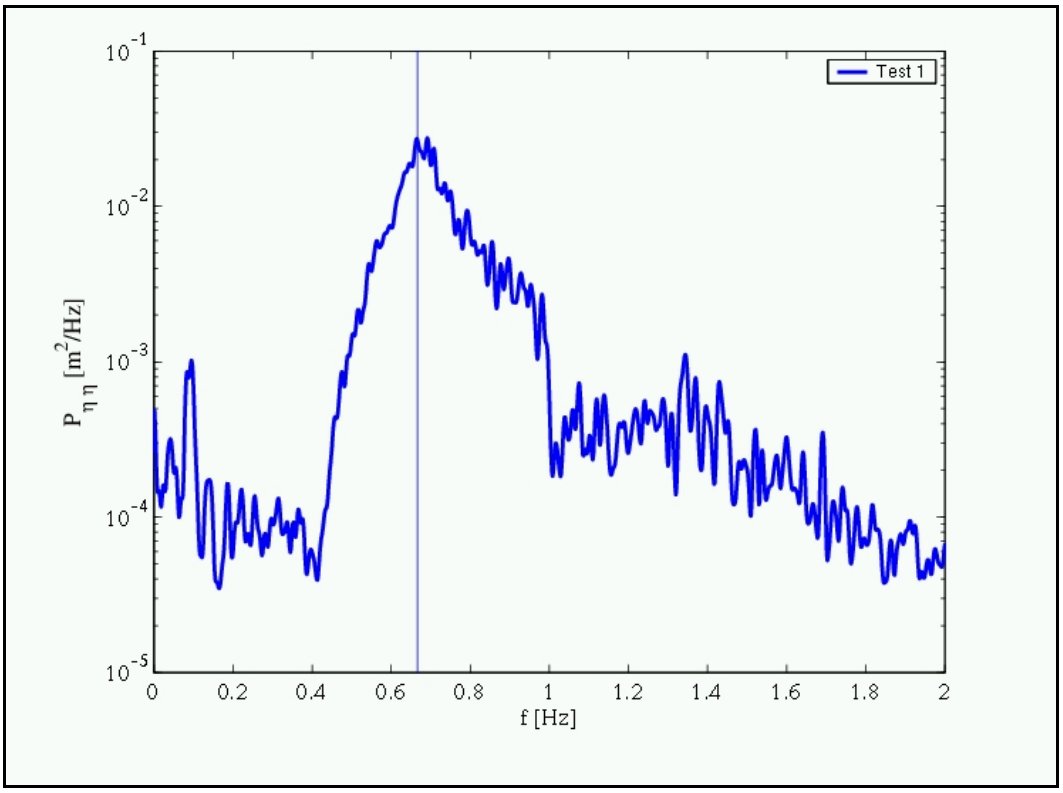

Figure 4. Power spectral density of the free surface seaward of breaker region, at measurement location 10 m.

The cross-shore distribution of wave heights is shown in Figure 5. Note that an analysis including the full spectrum of frequencies results in increased H_{rms} near the shoreline. Due to the large number of transects, data from only half of the alongshore measurement positions are shown (y = 16, 20, 24, 28, and 32 m), and a measure of the longshore uniformity in wave heights can be judged from the degree of scatter in the alongshore direction.

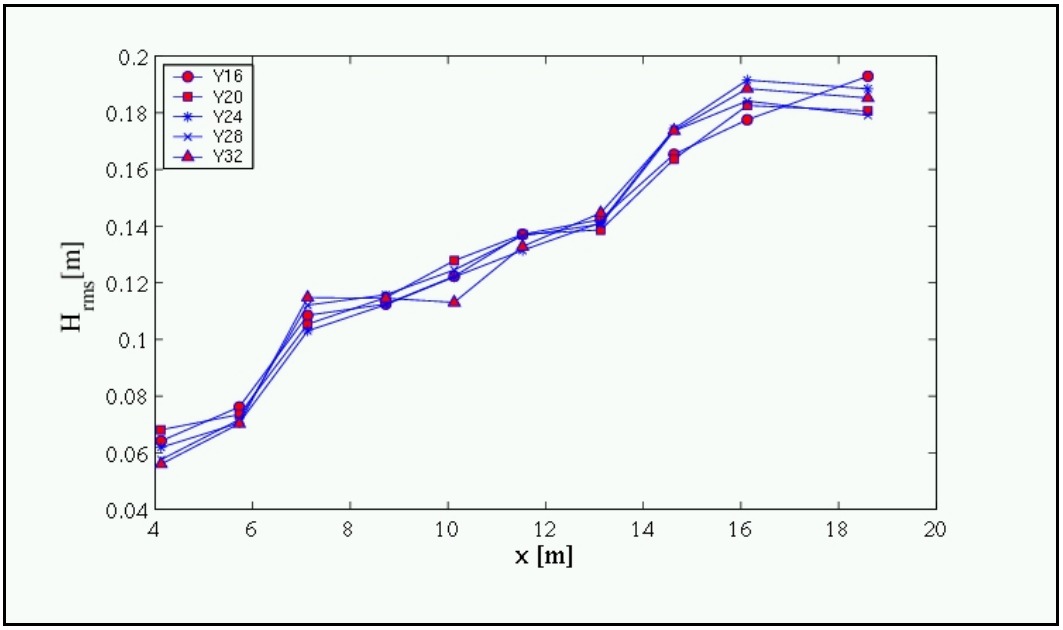

Figure 5. Cross-shore distribution of wave height at transects *y* = 16, 20, 24, 28, and 32.

LSTF currents

Time-averaged longshore velocities at the same transects are shown in Figure 6 where current magnitudes are measured at one-third of the water depth above the bottom. With exception of the most shoreward and most seaward measurement locations, the standard deviation of the velocities measured between transects was less than 1 cm/s. The cross-shore distribution of longshore current velocity showed a sharp increase in velocity within the breaker region. The region extending from the outer surf zone to the still-water shoreline is characterized by a broad, nearly-uniform velocity profile with the highest measured velocities occurring in the shallowest region. Currents within the swash zone shoreward of ADV1 were not systematically measured during these tests. Visual observations of injected dye indicate large alongshore velocities near the shoreline. The longshore current direction at the most seaward gauge 10 reverses direction (Figure 6). This recirculation current is the undesirable artifact of the finite length of the basin, and may have influenced the distribution of the current, particularly in the outer surf zone.

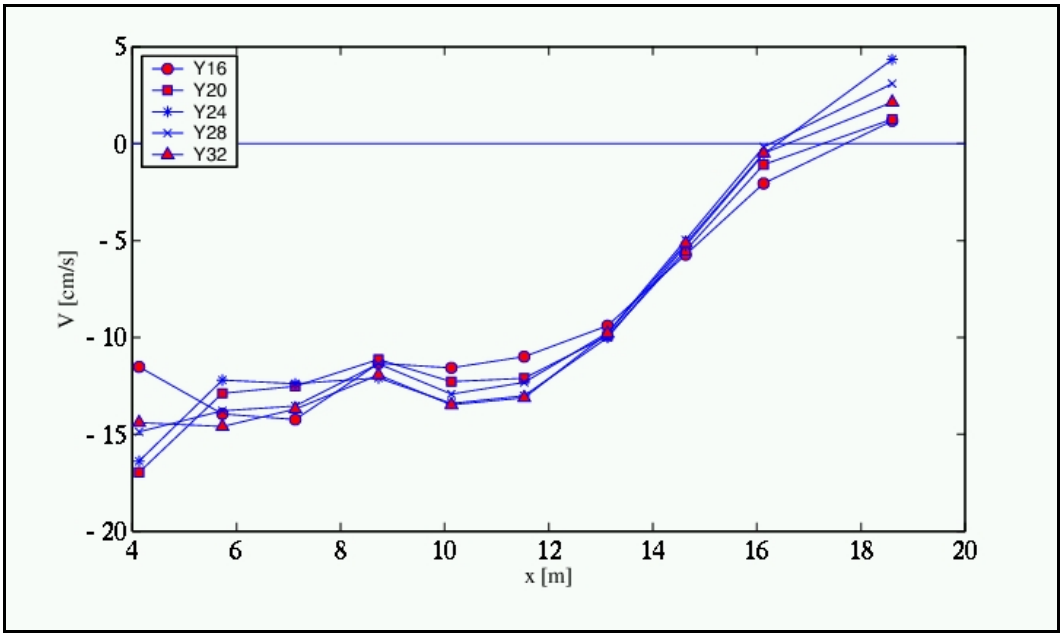

Figure 6. Cross-shore distribution of longshore current based on measurements at $z = -2d/3$ for transects y = 16, 20, 24, 28, and 32 m.

3 Nearshore Momentum Balance

The nearshore momentum balance includes momentum fluxes due to waves, turbulent mixing, and bottom shear stresses. Each of these will be discussed in the following sections.

Momentum fluxes due to waves

It is now well understood that associated with an organized wave motion is a momentum flux that is proportional to the energy flux (e.g., Longuet-Higgins 1970). Outside of the breaking wave region, for the majority of random seas, energy gradients are small and changes in the momentum flux are negligible. In the surf zone, however, the loss of energy due to wave breaking generates a force on the water column that is typically a primary term in the momentum balance. At the simplest level, any phase-averaged depth-integrated model can incorporate the effects of wave momentum flux by utilizing linear theory to describe fluid velocities and pressures and averaging over a representative wave period. The resulting 2-D stress tensor, typically termed radiation stresses (e.g., Dean and Dalrymple 1992), is

$$S_{xx} = E\left\{\frac{c_g}{c}\left(\cos^2\alpha + 1\right) - \frac{1}{2}\right\} \tag{1}$$

$$S_{yy} = E\left\{\frac{c_g}{c}\left(\sin^2\alpha + 1\right) - \frac{1}{2}\right\} \tag{2}$$

$$S_{xy} = E\frac{c_g}{c}\sin\alpha\cos\alpha \tag{3}$$

$$E = \frac{1}{8}\rho g H_{rms}^2 \tag{4}$$

where ρg is the unit weight of water, c_g is the group speed, c is the phase speed, and α is the angle of wave propagation, all based on the spectral peak. Johnson and Smith (2005) concluded that the the off-diagonal stress S_{xy} was significantly over-predicted by the linear expression in Equation 3. However, no viable alternative formulation is presently available. It should

be noted that it is possible to include the effect of the detached and aerated region of intense energy dissipation known as the roller (Reniers and Battjes 1997) into the expression for radiation stress. Ruessink et al. (2001), for instance, showed that inclusion of a roller contribution in the momentum balance improves the estimates of the cross-shore distribution of longshore current on barred beaches. Rollers have little influence on the overall wave forcing in the surf zone, but change the spatial distribution (generally shifting the peak current toward the shoreline).

Even in fully 3-D models, wave stress is typically applied only at the surface (e.g., Lesser 2004). Strictly speaking, only the roller contribution can be applied near the surface exclusively. A depth-dependent forcing can be derived that remains consistent with the widely applied linear representation:

$$s_{xx} = \frac{E2k}{\sinh 2k\bar{h}}\left(\cosh^2 kz' \cos^2 \alpha - \sinh^2 kz'\right) + \frac{E}{2\bar{h}} \tag{5}$$

$$s_{yy} = \frac{E2k}{\sinh 2k\bar{h}}\left(\cosh^2 kz' \sin^2 \alpha - \sinh^2 kz'\right) + \frac{E}{2\bar{h}} \tag{6}$$

$$s_{xy} = \frac{E2k}{\sinh 2k\bar{h}}\left(\cosh^2 kz' \sin\alpha\cos\alpha\right) \tag{7}$$

where k is the wave number, $\bar{h}$ is the slowly-varying water depth, and z' is a local vertical coordinate system with $z' = 0$ at the bottom. Integration of Equations 5-7 from the bottom to the mean water line yields the expressions in Equations 1-3, e.g., $\int_0^h s_{xx}\, dz' = S_{xx}$.

In the nearshore environment, the component of radiation stress s_{yy} typically has small alongshore gradients, and is expected to be less important than the other two components. For small wave incidence angles $\cos\alpha$ is well approximated by one, and given the identity $\cosh^2 kz - \sinh^2 kz = 1$, the cross-shore radiation stress s_{xx} is uniform over depth. On the other hand, the off diagonal component s_{xy} demonstrates the largest variation with depth.

The vertical variation of the cross-shore velocities σ_u^2 variance , which is proportional to s_{xy} , is shown in Figure 7 for the lab data. When compared with steady current velocity profiles, measurements taken near the bottom reveal that the effect of the boundary on wave-induced velocities is confined to a relatively thin layer near the bed. The large near-bottom gradient in the magnitude of oscillatory velocity compared to steady current velocities is consistent with the extensive literature pertaining to wave and current boundary layers (e.g., Grant and Madsen 1979). Outside of the thin boundary layer but near the bottom, velocities have little variation with depth, in accordance with the cosh dependence of linear waves. Figure 7 indicates that simple depth-invariant forcing is a reasonable assumption. Furthermore, the depth-variation is smaller than the discrepancy between measurements and the wave-orbital velocity magnitudes predicted by linear theory as demonstrated in Johnson and Smith (2005). The degree of depth-variation is readily shown to be a function of wave number and depth, and a rational indicator of the error incurred in using the depth-invariant radiation stress is expressed as:

$$\varepsilon_{rms} = \left\{ \frac{1}{h} \int_0^h \left(\frac{s_{xy} - S_{xy}/h}{S_{xy}/h} \right)^2 dz' \right\}^{\frac{1}{2}} \tag{8}$$

Figure 8 shows the root-mean-squared error in the organized wave forcing over the depth of the water column. The error is negligible in the shallow-wave (surf zone) environment. Significant deviations occur in the intermediate and deeper water case. In restricting the scope to the nearshore region where radiation stress gradients are important, it is justifiable to use a simple depth-invariant forcing in 3-D flow field development.

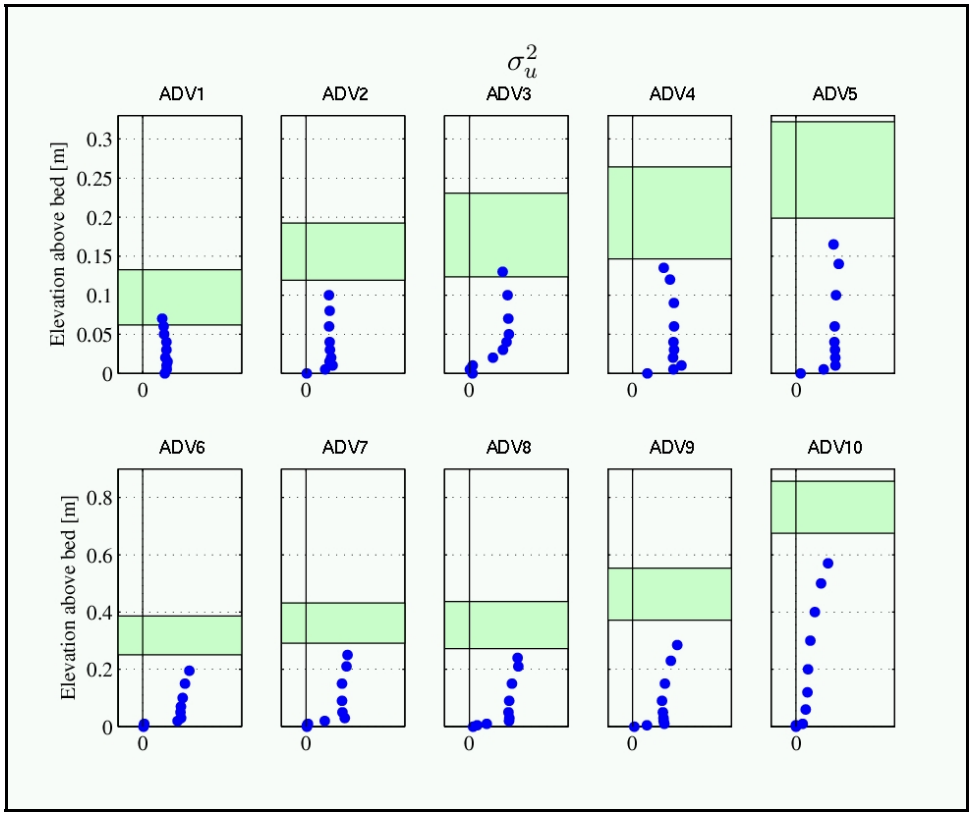

Figure 7. Depth-variation of wave-induced variance.

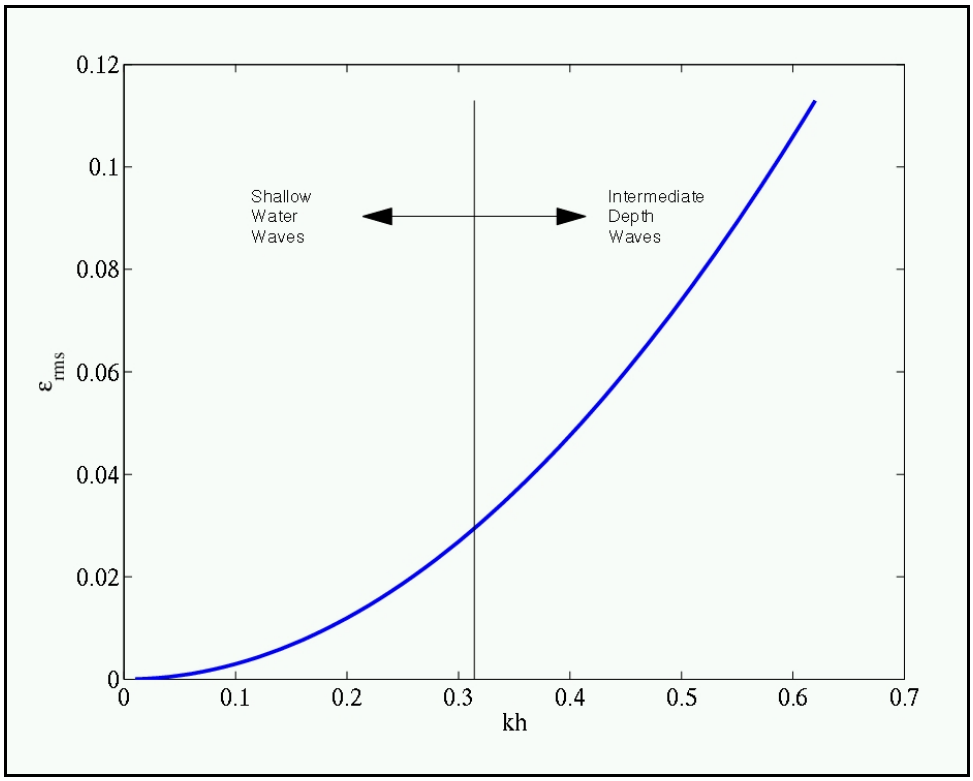

Figure 8. Error incurred in using depth-invariant radiation stress.

It should be emphasized that within the surf zone, significant departures from the linear representation of hydrodynamics have been demonstrated (Johnson and Smith 2005, Stive 1980). Furthermore, the depth-dependent Equations 5–7 have only been verified in the prediction of bulk hydrodynamics such as wave-induced setup and depth-averaged longshore current. The use of the inviscid wave stresses while neglecting the turbulent roller and near surface energy dissipation is deemed inappropriate in the computation of undertow profiles. For instance, Xia et al. (2004) used linear wave theory to predict the cross-shore current field that exhibited seaward-directed flow near the trough level and landward-directed flows near the bed. The stark contrast of these predictions with the established theoretical understanding, experimental and field data make clear the problem of using simplified depth-dependent stresses in the nearshore region. As an alternative, it is proposed subsequently that a local mass balance is used with a single boundary condition, thus avoiding some of the complexity of the stress distribution while still developing realistic profiles.

Bottom shear stress

The bottom shear stress due to combined waves and currents are of primary importance in the determination of the magnitude and depth-dependence of the currents in the nearshore region. In uniform open channel flow, the bottom shear stress is simply deduced from the hydraulic gradient. In a nearshore environment, however, it is more complicated to assess. Laboratory studies of bottom shear offer the opportunity to collect detailed hydrodynamic data in a controlled environment, but are typically restricted to colinear waves and currents. Field studies are conducted with waves and currents at arbitrary angles, but these investigations suffer the complexities of bathymetric nonuniformities, wind stress, tidal fluctuations, longshore pressure gradients, and data paucity (e.g., Thornton and Guza 1981, Feddersen et al. 1998, among others). The LSTF affords the opportunity to examine the bottom stress with waves and currents propagating at large angles under carefully controlled conditions.

The measured longshore forcing due to waves and currents in the LSTF were compared with several models for bottom shear stress utilizing measured hydrodynamics and bed forms. The analysis of Johnson and Smith (2005) populates the terms in the alongshore momentum balance with detailed measurements from a laboratory experiment and leaves the bottom shear stress as the residual. The inferred stress acts as the stan-

dard used to assess the several models in the surf zone. The quadratic drag law is applied using measured hydrodynamics and several different friction factor formulations. The wave and current interaction model of Grant and Madsen (1979), commonly applied on the continental shelf, is used here with the roughness parameterization of Wikramanayake and Madsen (1994) to compute the stress.

Alongshore momentum balance

It is well understood that the cross-shore decay in wave height and radiation stress generates longshore currents and wave setup (e.g., Longuet-Higgins 1970). While many problems must be treated in two horizontal dimensions, the laboratory design and measured data justify the assumption of alongshore uniformity in the presence of a longshore current. By collapsing this problem to one dimension, the alongshore momentum balance is simplified considerably, especially because direct measurements of pressure are rendered unnecessary. With an assumption of statistically independent wave and turbulent motions, the stresses due to the interaction of wave and turbulent velocities are neglected. After depth-averaging and time-averaging along with the application of boundary conditions, the longshore momentum equation is expressed as:

$$\overline{\rho \frac{\partial}{\partial x} \int_{z_b}^{\eta} uv \, dz} = \overline{\rho \frac{\partial}{\partial x} \int_{z_b}^{\eta} \tau_{xy} \, dz} - \overline{\tau_{b_y}} \tag{9}$$

where ρ is the density of water, x is the cross-shore coordinate defined positive offshore, z is the vertical coordinate with $z = 0$ at the still-water-level and z_b is the bottom position, η is the instantaneous free-surface position, u and v are the combined wave and current velocities in the cross-shore and longshore direction, respectively, τ_{xy} represents the turbulent momentum flux, and τ_{by} is the bottom shear stress. The over-line indicates time-averaging, where the averaging interval is hundreds of wave periods for this study involving irregular waves.

The first term in Equation 9 represents the total forcing for the longshore current due to the organized oscillatory wave motion, the interaction of the steady currents, and a roller contribution. Data collected along the single transect shown in Figure 3 with 10 measurement locations over the vertical are used to quantify the total forcing. The analysis is detailed in Johnson and Smith (2005).

While the analytical solution of Longuet-Higgins (1970) required the lateral mixing term τ_{xy} to predict physically realistic longshore current distributions, subsequent studies have demonstrated little effect when including this term for irregular waves. For instance, Thorton and Guza (1986) concluded that the lateral mixing was not needed to match measured field data of currents and irregular waves, and Feddersen et al. (1998) found that the turbulent momentum flux was small relative to the bottom shear stress. Thus, given the evidence of a small contribution, coupled with the difficulties in estimating Reynolds stresses from ADV measurements, the effect of lateral mixing is neglected.

Bottom shear stress formulations

By neglecting the turbulent momentum flux in Equation 9, bottom shear stress is left as the sole balance for the cross-shore gradient in momentum flux. A great deal of effort has gone into the exploration of bottom shear stress models (e.g., Nielsen 1992, and many others) as the primary impedance force in the alongshore momentum balance. Small-scale vortex ripples have a primary effect on the rate at which momentum is shifted from the fluid to the bed. Ripples such as seen in Figure 2 act to increase the shear stress for a given free-stream wave and current velocity. Alternatively, for a given shear stress, the presence of ripples acts to reduce the magnitude of the current. The physical roughness is the length that scales the flow variation in the vertical. In the absence of bed forms, the relevant scale is the grain diameter. The wave generated vortex ripples, however, are much larger than the grain length scale, and the roughness is less directly defined. Most shear stress models require a roughness estimate, and the roughness model developed in conjunction with the stress model should be used.

Considering the difficulty in determining the stress from first principles, the quadratic friction law remains widely used for both steady and oscillatory flows, and is written:

$$\overline{\tau_{b_y}} = \rho c_f \, \overline{v\sqrt{u^2 + v^2}} \tag{10}$$

where c_f is a drag coefficient. This formulation for stress is an empirical result based on steady flow but is, nevertheless, commonly applied in time-dependent models. Several studies have indicated the suitability of the quadratic model (Equation 10) in the nearshore region, but examina-

tion of the alongshore-oriented shear stress has been limited to field studies. Feddersen et al. (1998) showed a correlation between the combined wind and wave forcing and the bottom friction based on a quadratic friction formulation. Trowbridge and Elgar (2001) concluded that the quadratic drag law was accurate for energetic conditions by comparisons with the measured near-bottom turbulent Reynolds shear stress. At a smaller time-scale, the time-dependent shear stress determined from measurements in a flume and presented by Cox et al. (1996) was faithfully described by the quadratic law.

Shear stress can be computed with Equation 10 using measured values of velocity and time-averaging over the total time series. Such estimates of τ_{by}, however, are dependent on the single vertical position used for collection of u and v. The distance from the bed should be small relative to the water depth, but also well above the local influence of bed forms. To demonstrate the depth-dependence of shear stress divided by the drag coefficient $\tau_{by}/c_f = \rho v\overline{\sqrt{u^2+v^2}}$, the total measured velocities at each vertical location are used to develop an estimate of the shear stress as shown in Figure 9. For reference, the shaded region shown on each plot depicts the range of the root-mean-square wave height H_{rms} centered about the measured mean water level. For a given constant drag coefficient, the computed shear stress was 10-15 percent larger using velocities at the midpoint of the still-water depth when compared to the stress from a location one-third of the depth from the bottom. This difference is not significant relative to the scatter of friction factors, and the quadratic-based bottom shear stress was computed using the time series of velocities measured at a distance of one-third of the depth from the bottom hereafter.

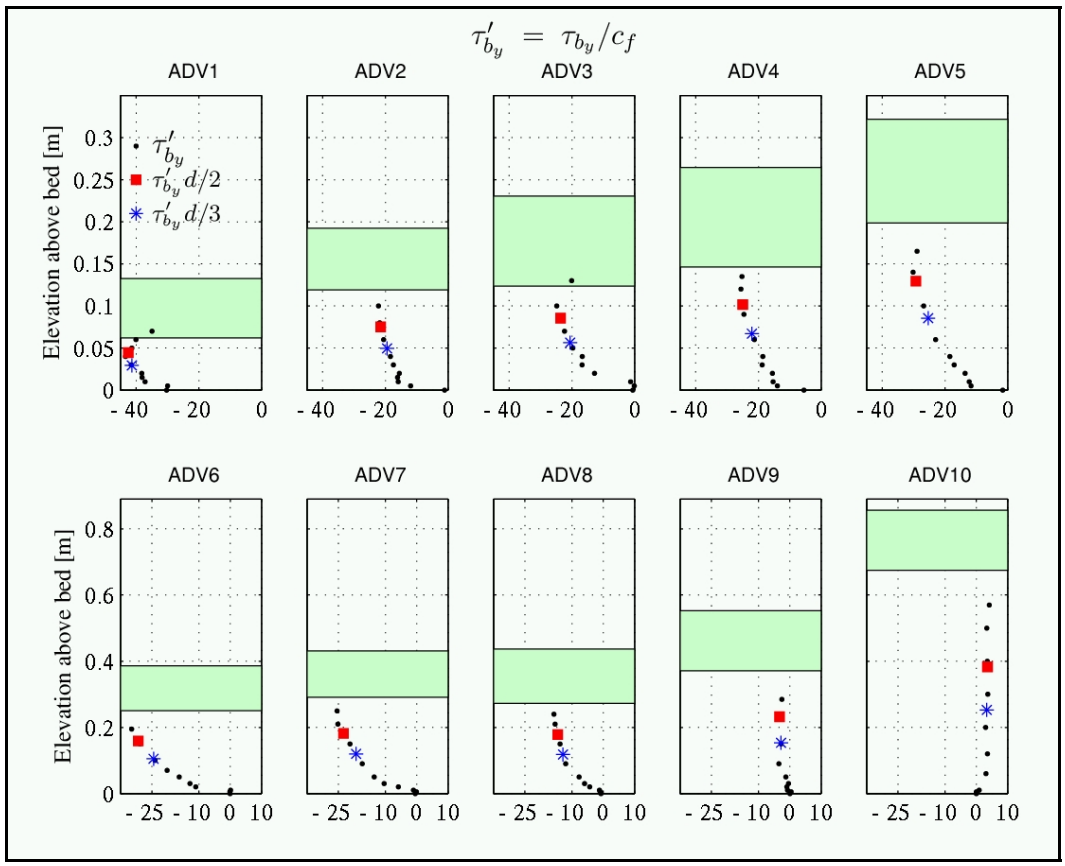

Figure 9. Variation of stress estimates over depth.

Many models use a simple constant coefficient of friction, without regard for variations in water depth, wave effects, or bottom roughness. Feddersen et al. (1998) found that the momentum balance closure was statistically improved by using different coefficients for regions inside and outside of the surf zone. The region of study in this laboratory investigation was primarily inside the surf zone, and a single value of c_f is used initially.

Thornton and Guza (1981) estimated the coefficient within the surf zone at Torrey Pines Beach, CA, over several days and found considerable scatter, but computed an average value of $c_f = 0.01$. Figure 10 shows that the computed stress for the LSTF case according to the quadratic law with a constant coefficient compares well to the inferred shear stress (depicted as a solid line) over the surf zone except at ADV1 where the stress is overpredicted.

The model based on a Manning's factor is empirically founded on open channel flow, but is nevertheless used in nearshore computations (e.g., Smith et al. 1993). The relation between Manning's n and c_f in SI units yields a friction coefficient with a weak variation with depth:

$$c_f = \frac{gn^2}{h^{1/3}} \tag{11}$$

where g is acceleration due to gravity and h is the mean water depth. Smith et al. (1993) concluded that $n = 0.02$ resulted in an optimal fit of computed longshore currents to measured field data. Figure 10 shows that stress based on $n = 0.02$ is about 50 percent of the forcing over most of the surf zone for the LSTF case.

For hydraulically rough flow, the Manning-Strickler law is often used in open channels.

$$c_f = 0.015\left(\frac{r_a}{h}\right)^{1/3} \tag{12}$$

where r_a is the apparent roughness length scale which is increased from the current-only conditions due to the presence of waves (Grant and Madsen 1979). There is no consensus on a suitable roughness model in a nearshore environment over ripples, and in developing the shear stress based on Equation 12, r_a is based on the fitted log profiles that are presented subsequently. As seen in Figure 10, the Manning-Strickler based shear stress compares well with the forcing for the outer surf zone, but is only about half of the forcing in the inner surf zone.

The wave friction factor, on the other hand, is based on laboratory data of purely oscillatory flow, in the absence of currents. The LSTF presents a case of a combined wave and current environment where, in a strict sense, the wave-friction factor is not applicable. However, the bottom stress in the nearshore environment is typically dominated by the wave effects, and one wave-friction factor formulation is included herein without accounting for the interaction.

$$\overline{\tau_{b_y}} = \rho\frac{f_{cw}}{2}\overline{v\sqrt{u^2+v^2}}; \rho\frac{f_w}{2}\overline{v\sqrt{u^2+v^2}} \tag{13}$$

where f_{cw} is a wave-current friction factor and f_w is a wave friction factor. The wave friction factor is considered to be a function of the wave-Reynolds number $Re = U^2/(\omega\nu)$ and the relative bed roughness r/A where U is the velocity amplitude, ω is the radian frequency, ν is kinematic vis-

cosity, r is roughness length scale, and A is orbital amplitude of the fluid motion above the boundary layer (e.g., Nielsen 1992). With the exception of the most shoreward measurement location and the most seaward measurement location, the flow is classified as fully rough turbulent flow with values of the $\frac{v_* r}{\nu} > 70$ where v_* is the shear velocity in the longshore direction. The wave friction factor is then considered to be independent of Re and a function of relative roughness only. There exist many formulations for the wave friction factor, and the single presented example of results is based on Equation 1.2.23 in Nielsen (1992) and is within ~20 percent of the models of Swart (1974) and Soulsby (1997).

$$f_w = \exp\left[5.5\left\{\frac{r}{A}\right\}^{0.2} - 6.3\right] \tag{14}$$

The roughness model developed in conjunction with Equation 14 is attributed to skin friction, a form drag, and the effects of momentum loss due to moving sand grains:

$$r_{Grain} = 2.5 d_{50} \;\; ; \;\; r_{Form} = 8\frac{\eta_r^2}{\lambda_r} \;\; ; \;\; r_{moving} = 5\theta_{skin} d_{50} \tag{15}$$

where d_{50} is the median grain size, η_r is the ripple height, λ_r is the ripple length, and θ_{skin} is the grain roughness Shields parameter. Figure 10 shows that the resultant shear based on a wave friction factor is about twice as large as the forcing.

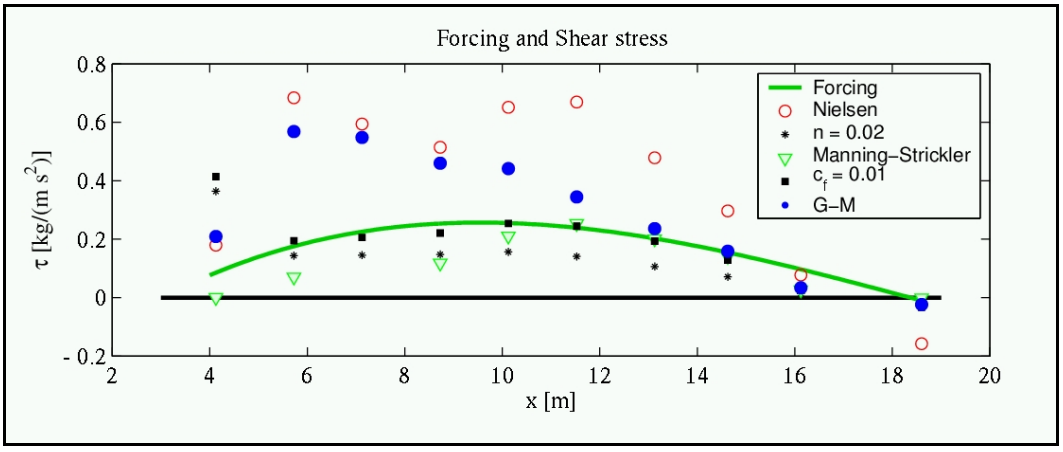

Figure 10. Cross-shore distribution of shear stress.

The wave and current interaction model of Grant and Madsen (1979) represents an accepted basis for the computation of bottom shear stress on the continental shelf. The model results presented herein include the modifications to the original formulation presented in Madsen (1995) and Madsen and Salles (1999) (G-M hereafter). The model for the eddy viscosity within the boundary layer directly includes interaction through a wave-current shear velocity u_{*wc} while outside of the boundary layer the effect is included implicitly through the matching conditions and an increased apparent roughness.

$$\overline{\tau_{b_y}} = \rho \nu_t \frac{\partial \bar{v}}{\partial z} = \begin{cases} \rho \kappa u_{*wc} z' \dfrac{\partial \bar{v}}{\partial z} & \text{for } z' < \delta_{wc} \\ \rho \kappa u_{*c} z' \dfrac{\partial \bar{v}}{\partial z} & \text{for } z' > \delta_{wc} \end{cases} \tag{16}$$

where ν_t is a turbulent eddy viscosity, κ is the von Kármán constant, z' is a local coordinate system with $z' = 0$ at the bottom, and δ_{wc} is the thickness of the wave-current boundary layer. The linear eddy viscosities assumed in Equation 16 are based on the shear production of turbulence only and do not account for the important wave breaking-induced turbulence. Cox and Kobayashi (2000), however, presented data indicating that intermittent turbulence caused by breaking waves was an order of magnitude larger than the shear-generated turbulence near the bottom. Nevertheless, the results of the G-M model are presented here without modifications. The physical roughness constitutes the only free parameter, and the simple model for 2-D equilibrium ripples presented by Wikramanayake and Madsen (1994) is used: $k = 4\eta_r$. The conspicuous lack of a slope dependence is explained by the many data sets demonstrating that the ratio of ripple height to wavelength measured in natural sand beds is nearly constant. Figure 11 shows the magnitude (including cross-shore) of measured and predicted current profiles at the 10 cross-shore measurement locations. Measurements of $\bar{v}$ at ADV3 were considered to be unreliable, and therefore are not included in the comparisons. Note that the significant gradient in the current profile near the surface is due to the inclusion of the cross-shore currents. The vertical position of the boundary layer is the location of discontinuity in slope evident in the G-M current profile, and is shown in Figure 11 as a dashed horizontal line. The reference current used as part of the solution procedure is located at twice the boundary layer thickness from the bed, and is depicted as a solid circular marker.

The current prediction is reasonable at the five deeper locations (ADV6-ADV10). Within the inner surf zone, however, the vertical gradient of the current is underpredicted inside of the boundary layer and overpredicted outside of the boundary layer. Figure 10 shows that computed shear stress is about twice as large as the forcing. This departure from the G-M theory is perhaps due to a roughness model that is not calibrated with data from inside of the surf zone, the turbulent production from wave breaking, or the pronounced effects of the shoreward-directed return current.

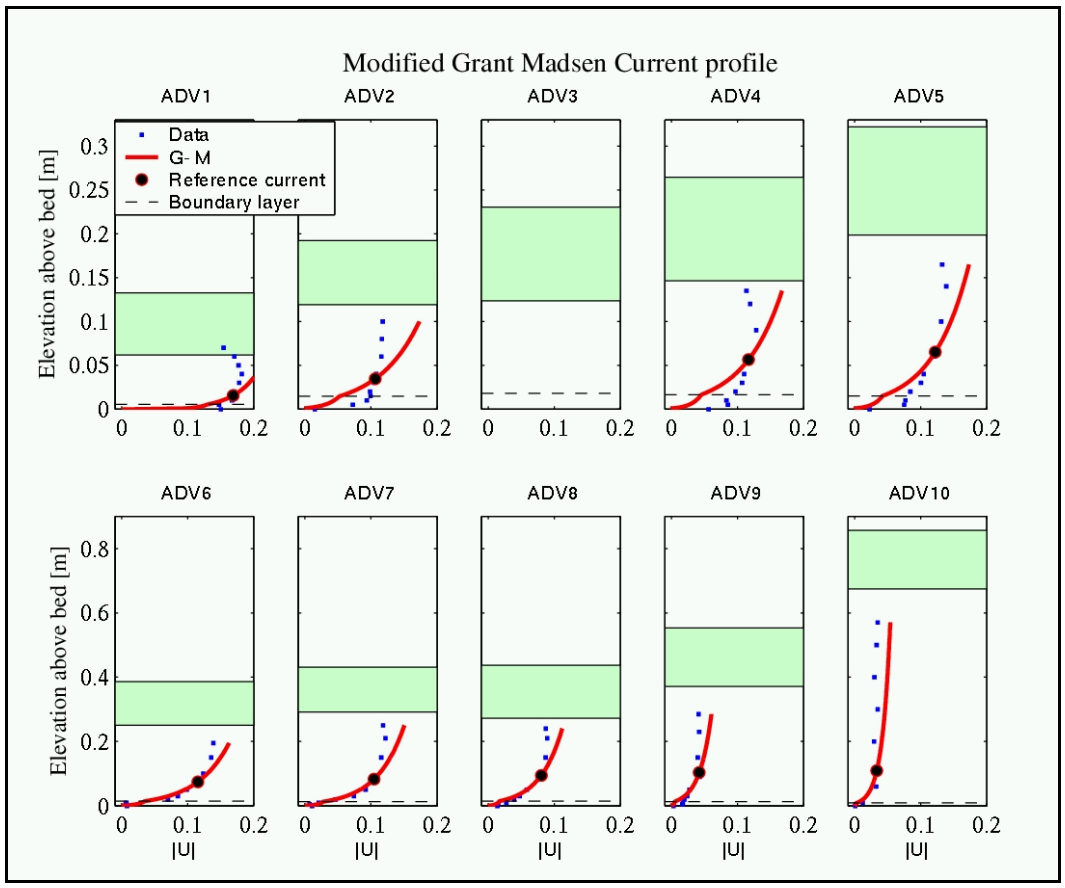

Figure 11. Measured and predicted longshore current profiles at 10 cross-shore locations.

Including wave-orbital velocities in stress estimates

Shear stress comparisons benefit from the use of measured currents and wave-orbital velocities. This detailed information is, of course, unavailable in the routine application of phase-averaged models. The unfortunate reality is that the simplifying assumption of small wave-induced velocities relative to the currents is commonly used as a result. Neglecting the wave-component of the shear is justifiable on the shelf, but the bottom stress in the nearshore region is significantly altered by the waves. A practical solu-

tion for including wave effects in the shear stress was presented by Nishimura (1982), termed the square-wave method. The shear stress deduced from the laboratory data is compared with the wave-neglecting simplification and the square-wave method. As mentioned previously, wave-velocity is often discounted in the computation of shear:

$$\overline{\tau_{b_x}} = \rho c_f \, \bar{u} \sqrt{\bar{u}^2 + \bar{v}^2} \quad ; \quad \overline{\tau_{b_y}} = \rho c_f \, \bar{v} \sqrt{\bar{u}^2 + \bar{v}^2} \tag{17}$$

where only the slowly-varying phase-averaged velocities $\bar{u}, \bar{v}$ are taken into account. The obvious effect of this simplification is a persistent underestimation of the shear stress, or alternatively, an overestimation of the nearshore current magnitude for a given hydrodynamic forcing. Nishimura (1982) approximated the wave-orbital velocities with a square-wave representation, and developed the simple analytical expression for the shear stress as follows:

$$\overline{\tau_{b_x}} = \rho c_f \left\{ \bar{u} \left(W + \frac{w_b^2}{W} \cos^2 \alpha \right) + \bar{v} \frac{w_b^2}{W} \cos\alpha \sin\alpha \right\}$$

$$\overline{\tau_{b_y}} = \rho c_f \left\{ \bar{v} \left(W + \frac{w_b^2}{W} \sin^2 \alpha \right) + \bar{u} \frac{w_b^2}{W} \cos\alpha \sin\alpha \right\}$$

$$w_b = \frac{\omega H_{rms}}{\pi \sinh k\bar{\bar{h}}}$$

$$W = \frac{1}{2} \left\{ \sqrt{\bar{u}^2 + \bar{v}^2 + w_b^2 + 2w_b(\bar{u}\cos\alpha + \bar{v}\sin\alpha)} \right.$$

$$\left. \sqrt{\bar{u}^2 + \bar{v}^2 + w_b^2 - 2w_b(\bar{u}\cos\alpha + \bar{v}\sin\alpha)} \right\} \tag{18}$$

As a cursory examination into the accuracy of these simplified expressions, measured laboratory wave height is used to develop w_b, and $\bar{u}, \bar{v}$ are represented by measured currents. In Figure 12 the computed shear stresses given by Equations 17 and 18 are compared with the shear stress computed with the full velocity time series as outlined previously. The stress estimates based on the steady currents are in significant error with a consistent underprediction of the stress. Conversely, the square-wave approximation exhibits relatively small differences from the full representation

except in the cross-shore stress τ_{by} for ADV's 3 and 4, which exhibit 40 percent error. The small but consistent overprediction of the stress magnitude is attributable to the use of linear theory to determine wave-induced hydrodynamics from the measured wave heights, which has been demonstrated to overestimate the orbital velocities (Johnson and Smith 2005). Thus, the square-wave approximation is a reasonable assumption that provides significant improvement in the stress calculation compared to neglecting the wave contribution.

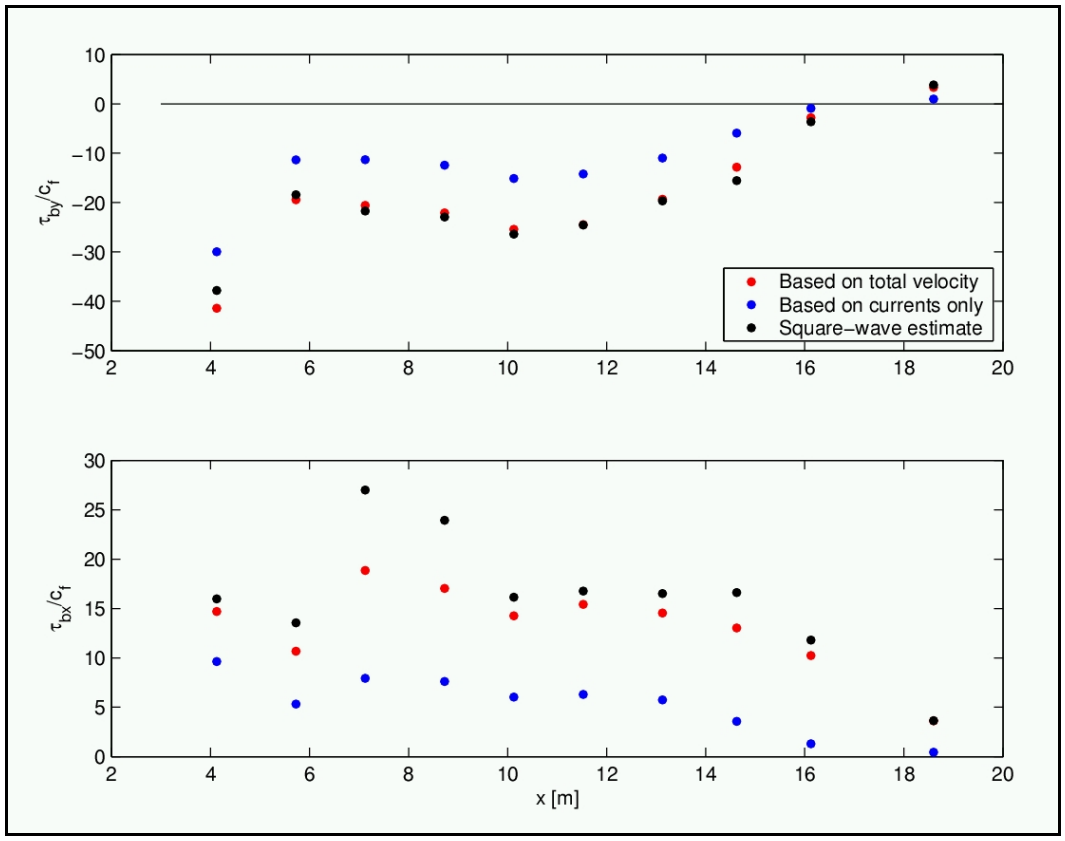

Figure 12. Shear stress estimates developed from full time velocity time series, steady currents only, and the square-wave approximation.

4 Depth Dependence of Currents

Determining the correct depth dependence of the nearshore current has been an area of active research for the past 20 years. In essence, an accurate description of the wave and current forcing, a suitable turbulence closure scheme, and boundary conditions are needed. The following section considers the simple one-way coupling where 2-DH solutions are used as a constraint when predicting the depth variation. The reality of 3-D flows, however, is that the depth variation can alter the 2-DH solution through enhanced mixing, contributions to the momentum flux, and a differing representation of the bottom shear stress. A prediction of the depth variation can, in theory, then be used to quantify the effect in a 2-DH solution using either an iterative approach or by using lagged depth-variation information from a previous time-step. Depth-integrated models that include the effects of a departure from depth-uniformity are termed quasi-3-D models (see Svendsen et al. (2002) for an example of a quasi-3-D nearshore model).

In the following, equations governing depth-variation will first be expressed as an implicit function of the 3-D current field, and then simplified to yield an explicit expression dependent on only the 2-DH variables. In the majority of nearshore domains, the implicit dependence is small. Complex problems with hydrodynamic variables that change rapidly in time and space, however, may violate the assumptions necessary for the simplification, and the resulting solution may be in error. Applications to complex environments such as rip channels should include additional representative calculations where, through iteration, the full 3-D field is developed and compared with the simplified solution. Finally, to introduce an efficient and uncomplicated procedure to predict depth dependence, an assumed depth profile is subject to constraints and boundary conditions, and compared with the more detailed stress-resolving solution.

The procedure outlined here is based on the specification of a shore-normal coordinate system with a rotation angle between the local system and the 2-DH system of β as shown in Figure 13.

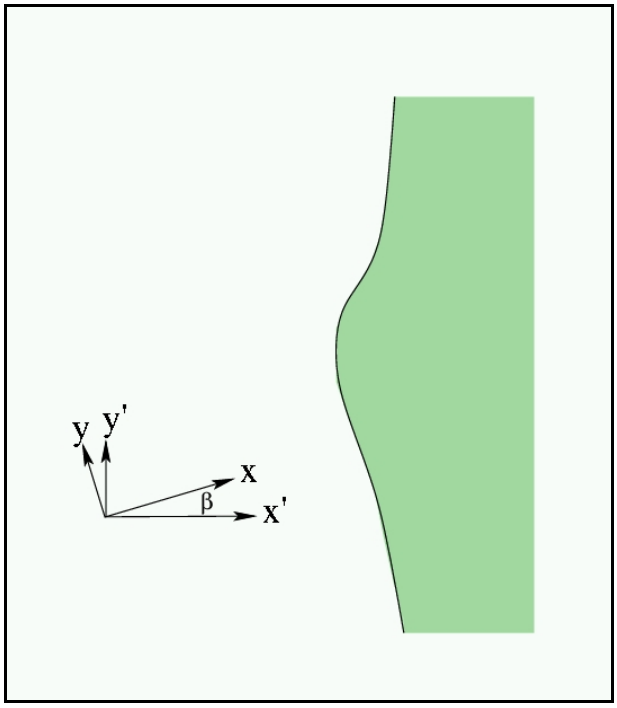

Figure 13. Local and 2-DH coordinate systems.

The general relations governing the vector $\vec{s}$ components are given by

$$s_x = s_{x'} \cos\beta + s_{y'} \sin\beta$$

$$s_y = -s_{x'} \sin\beta + s_{y'} \cos\beta$$

$$s_{x'} = s_x \cos\beta - s_y \sin\beta$$

$$s_{y'} = s_x \sin\beta + s_y \cos\beta$$

where primed variables are in the 2-DH domain and unprimed variables are the local system.

Shore-normal currents

A prediction of the depth-variation of the slowly varying currents requires an examination of the depth-dependent Reynolds equations. The phase-averaged cross-shore momentum equation including the inertial terms is expressed as follows:

$$\frac{\partial \bar{u}}{\partial t}+\frac{\partial \bar{u}^2}{\partial x}+\frac{\partial \overline{\tilde{u}^2}}{\partial x}+\frac{\partial \bar{u}\,\bar{v}}{\partial y}+\frac{\partial \overline{\tilde{u}\tilde{v}}}{\partial y}+\frac{\partial \overline{\tilde{u}\tilde{w}}}{\partial z}=-\frac{1}{\rho}\frac{\partial P}{\partial x}+\frac{\partial}{\partial z}\left\{\nu_t\frac{\partial \bar{u}}{\partial z}\right\} \tag{19}$$

where x is a local coordinate system directed onshore; y is a local longshore coordinate; z is the vertical coordinate, positive up; and P is the phase-averaged pressure. Cross-shore and longshore directed horizontal velocities u and v, respectively, and the vertical velocity w are decomposed into a into slowly-varying and wave-induced velocities

$$u=\bar{u}+\tilde{u} \quad ; \quad v=\bar{v}+\tilde{v} \quad ; \quad w=\bar{w}+\tilde{w} \tag{20}$$

Equation 19 includes the assumption that, in accordance with long-wave models, the steady vertical current $\bar{w}$ is negligible relative to the horizontal currents, shear stress is suitably parameterized with an Reynolds-type closure, and the cross-shore gradients of integrated turbulent shear are assumed to be small (Stive and Wind 1982). It is worth noting that Equation 19 is consistent with 2-DH long-wave models if, after depth integration, pressure is assumed to be hydrostatic and all products of time-varying components are expressed as radiation stresses.

The assumption of periodic waves of permanent form results in wave-induced horizontal and vertical velocities that are $\pi/2$ out of phase, and leads to a vanishing time-averaged $\overline{\tilde{u}\tilde{w}}$. Rivero and Arcilla (1995) argue that a bottom slope and a wave amplitude gradient render this simplification invalid. A simple expression for the vertical stress term was proposed, and is adopted herein:

$$\frac{\partial}{\partial z}(\overline{\tilde{u}\tilde{w}})=-\frac{1}{2}\frac{\partial}{\partial x}(\overline{\tilde{u}^2}-\overline{\tilde{w}^2}) \tag{21}$$

If the wave components are expressed according to linear theory:

$$\tilde{u}=\tilde{\eta}\omega\frac{\cosh k(z')}{\sinh k\bar{h}}\cos\alpha \quad ; \quad \tilde{v}=\tilde{\eta}\omega\frac{\cosh k(z')}{\sinh k\bar{h}}\sin\alpha \tag{22}$$

where $\tilde{\eta}$ is the wave component of the free-surface position, ω is the radian angular frequency, α is the local wave angle relative to the x-axis (local onshore direction), and z' is a local vertical coordinate with an origin at the top of the wave boundary layer. Substitution into Equation 19 yields:

$$\frac{\partial}{\partial z}\left\{\nu_t \frac{\partial \bar{u}}{\partial z}\right\} = \frac{\partial \bar{u}}{\partial t} + \frac{\partial \bar{u}^2}{\partial x} + \frac{\partial \bar{u}\,\bar{v}}{\partial y} + \frac{\partial}{\partial y}\left\{\frac{H_{rms}^2 \omega^2}{8} \frac{\cosh^2 kz'}{\sinh^2 k\bar{h}} \sin\alpha\right\}$$

$$+ g\frac{\partial \bar{\eta}}{\partial x} + \frac{1}{2}\frac{\partial}{\partial x}\left\{\frac{H_{rms}^2 \omega^2}{8\sinh^2 k\bar{h}}\right\} \tag{23}$$

where $\bar{\eta}$ is a phase-averaged free-surface position, $H_{rms} = \sqrt{8}\sigma$ and $\sigma =$ the standard deviation of the free-surface position. In Equation 23, $\cos\alpha$ is assumed to equal approximately 1 and pressure is assumed hydrostatic. Twice integrating in the vertical yields as follows:

$$\bar{u} = \overline{u_\delta} + \frac{1}{\nu_t}\int_0^z \int_0^z G_x \, dz \, dz$$

$$+ \frac{\partial}{\partial y}\left\{\frac{H_{rms}^2 \omega^2}{8k\nu_t} \frac{\sin\alpha}{\sinh^2 k\bar{h}}\left(\frac{\cosh 2kz'}{8k} + \frac{kz'^2}{4} - \frac{1}{8k}\right)\right\}$$

$$+ \frac{\tau_{bx}}{\rho\nu_t} z' + \frac{g}{2\nu_t}\frac{\partial \bar{\eta}}{\partial x} z'^2 + \frac{1}{4\nu_t}\frac{\partial}{\partial x}\left\{\frac{H_{rms}^2 \omega^2}{8\sinh^2 k\bar{h}}\right\} z'^2 \qquad z' > 0$$

$$G_x = \frac{\partial \bar{u}}{\partial t} + \frac{\partial \bar{u}^2}{\partial x} + \frac{\partial \bar{u}\,\bar{v}}{\partial y} \; \frac{\partial}{\partial t}\frac{Q_x}{\bar{h}} + \frac{\partial}{\partial x}\frac{Q_x^2}{\bar{h}^2} + \frac{\partial}{\partial y}\frac{Q_x Q_y}{\bar{h}^2} \tag{24}$$

where Q_x and Q_y are the cross-shore and longshore volumetric fluxes from the 2-DH model rotated to the local coordinate system, $\overline{u_\delta}$ is the near-bed current at the top of the wave boundary layer. The bottom phase-averaged shear stress τ_{bx} in Equation 24 is determined through an appropriate application of either the quadratic shear stress law or a more involved analysis as previously discussed.

In developing Equation 24, the eddy viscosity is assumed to be depth uniform, $\nu_t = .01\bar{h}\sqrt{g\bar{h}}$, considering the analysis presented in Svendsen et al. (1987) and the conclusion of Garcez Faria et al. (2000) that a depth-dependent eddy viscosity did not improve predictions of the undertow when compared with field data. It is precisely this assumption that limits the applicability of Equation 24 to the region outside of the wave boundary layer $z' > 0$. Equation 24 can be solved in the stated form by either using

an iterative technique or using lagged information for the velocities appearing in G_x. As mentioned previously, one possible approach for solving the implicit equation (Equation 23) is to employ the depth-uniform horizontal velocities from the 2-DH model, recognizing that the 2-DH solution variables may require rotation to conform to the local coordinate system. Then the depth-invariant form of G_x can be utilized, and all terms on the right-hand side of Equation 23 are known except the near-bed current at the top of the wave boundary layer $\overline{u_\delta}$. This free parameter is determined through an additional boundary condition or solution constraint. For instance, a no-slip condition was imposed by Svendsen et al. (1987), but it is inappropriate to extend a depth-uniform eddy viscosity formulation into the boundary layer. It is advised to use a statement of mass conservation whereby the total volume flux is imposed from both the 2-DH solution and a steady seaward-directed current under the trough level balancing the finite mass flux due to the presence of waves. Using the shallow-water approximation for the volume flux outlined in Kennedy et al. (1998), the local mass balance is expressed as follows:

$$\int_0^{d_t} \overline{u}\, dz' = Q_x \frac{d_t}{\overline{h}} - \frac{\sqrt{g\overline{h}}}{8}\left(\frac{H_{rms}}{\overline{h}}\right)^2 d_t \cos\alpha \tag{25}$$

where d_t is the depth from the edge of the boundary layer to the trough level, approximated as $d_t = \overline{h} - H_{rms}/2$. In effect, Equation 25 dictates that any wave-generated mass flux onshore is balanced locally by a seaward-directed current below trough level, and the applicability of such an assumption is not fully understood. Cases of slowly-varying shorelines, for instance, are consistent with Equation 25, but abrupt hydrodynamic or bathymetric changes in the longshore may introduce error. A deep rip channel in a nearshore bar, for instance, is a longshore nonuniformity that may make a local volume balance questionable. Surprisingly, even in this instance of highly irregular bathymetry, the predicted rip currents will likely not be in gross error. The primary mechanisms of rip current generation are longshore gradients in radiation stresses, wave-current interaction, and wave refraction/diffraction. Each of these effects is included in an accurate wave-driver coupled with a 2-DH model and are not dependent on depth variation of the currents. Generally a rip current magnitude will be O(1 m/s) and the wave-generated mass flux distributed over depth is typically O(0.1 m/s). Therefore, violations of the local balance assumption may contribute a small error and will not manifest as unreasonable

predictions. The use of Equation 25 as a constraint will produce results that are similar to other models that account for mass flux in a Generalized Lagrangian Mean reference frame (Lesser et al. 2004). The resulting expression for the near-bed velocity:

$$\overline{u_\delta} = \frac{Q_x}{\bar{h}} - \frac{\sqrt{g\bar{h}}}{8}\left(\frac{H_{rms}}{\bar{h}}\right)^2 \cos\alpha - \frac{G_x d_t^2}{6\nu_t}$$

$$-\frac{\partial}{\partial y}\left\{\frac{H_{rms}^2\omega^2}{8k\nu_t}\frac{\sin\alpha}{\sinh^2 k\bar{h}}\left(\frac{\sinh 2kd_t}{16k^2 d_t} + \frac{kd_t^2}{12} - \frac{1}{8k}\right)\right\}$$

$$-\frac{\tau_{bx}}{2\rho\nu_t}d_t + \frac{g}{6\nu_t}\frac{\partial\bar{\eta}}{\partial x}d_t^2 - \frac{1}{12\nu_t}\frac{\partial}{\partial x}\left\{\frac{H_{rms}^2\omega^2}{8\sinh^2 k\bar{h}}\right\}d_t^2 \tag{26}$$

where the depth-uniform version of G_x was used in the interest of brevity. The solution of Equation 24 along with Equation 26 constitutes a solution for the depth-dependent cross-shore currents from the edge of the wave boundary layer to the trough level using the bottom shear stress, a mass conservation statement, and momentum contributions due to the organized wave motion, described according to free-surface statistics.

In accordance with all boundary layer theories, the profile within the thin wave boundary layer is assumed to vary logarithmically. The thickness δ may be approximated with the expression of Grant and Madsen (1979)

$$\delta = C\frac{\kappa}{\omega}\sqrt{\frac{\tau_{max}}{\rho}} \tag{27}$$

where the maximum shear stress τ_{max} was introduced earlier, C is an empirical constant in the range of 1–2, and $C = 2$ is used herein. A match of currents at the boundary layer edge leads to the profile within the boundary layer:

$$\bar{u} = \frac{\bar{u}_\delta}{\ln\frac{30\delta}{k_n}}\ln\frac{30z}{k_n} \qquad \text{for} \qquad z < \delta \tag{28}$$

Figure 14 shows the depth-variation of the steady current velocities at the 10 cross-shore measurement locations. The shaded region in each plot de-

picts the range of the root-mean-square wave height H_{rms} centered about the measured mean water level. Data are shown as discrete symbols, and the modeled steady velocities are solid lines. The depth-varying cross-shore currents prescribed by this stress-resolving method, Equation 24 along with Equation 26, are shown as black lines, where the solid line accounts for the effect of the steady currents and the dashed line neglects the steady contribution, i.e., $G_x = \frac{\partial \bar{u}^2}{\partial x} : 0$. Clearly the effect of the steady currents on the depth variation is minimal as the traces are nearly identical. This is consistent with the conclusions stated previously that the steady effects on the depth-integrated solution are inconsequential. In short, $G_x = 0$ facilitates the solution of the depth variation and is a justifiable simplification.

It is important to note that the 2-DH model results would have computed a depth-averaged cross-shore current that reduces to zero in the steady-state case. If a simplified expression for the bottom shear stress were based only on $Q_x = 0$, the modeled undertow profiles would exhibit no slope near the bed. This result, of course, is not supported by the data, and highlights the need to include the depth-variation of the currents when computing the bottom shear stress and possibly supplying the corrected stress to the 2-DH model.

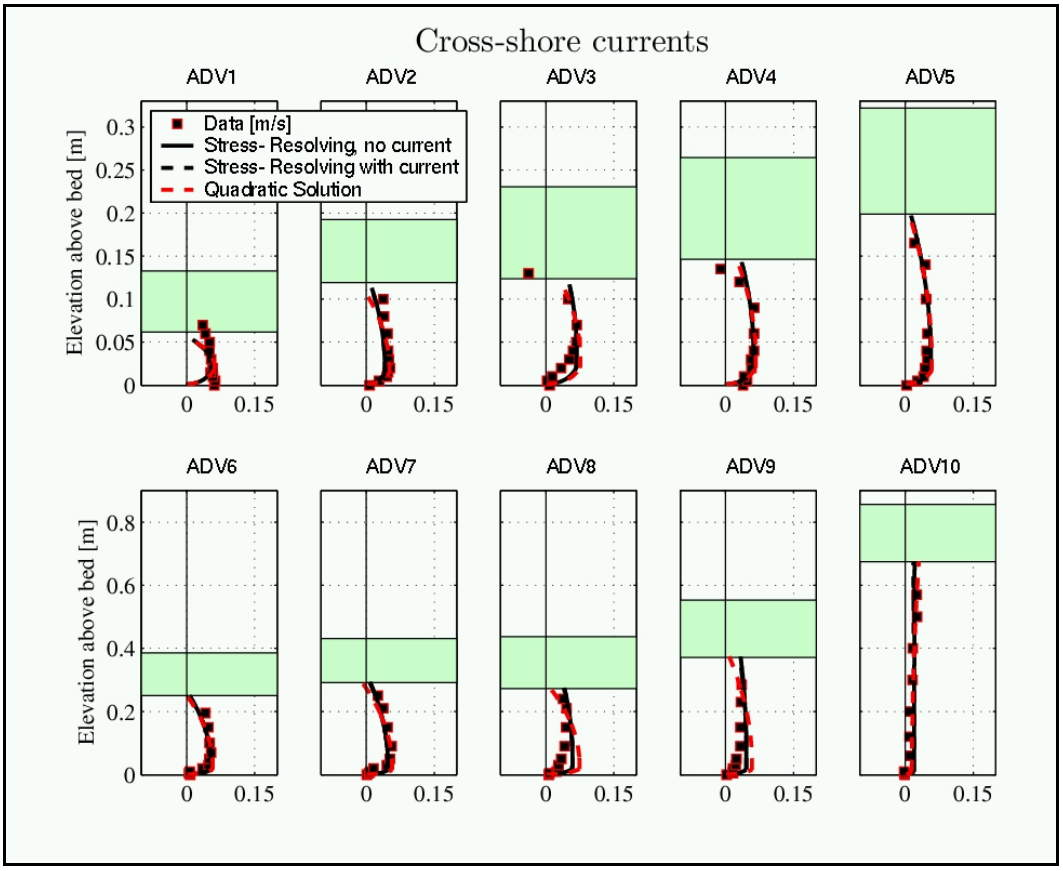

Figure 14. Depth-variation of cross-shore currents.

Shore-parallel flow

The details of the derivation of the shore-parallel flow are omitted here, but are analogous to the cross-shore analysis previously presented. One fundamental difference in boundary conditions is that wave-induced mass flux is absent from the volume balance statement, while an argument could be made that the waves may induce a small mass flux in the long-shore direction. Recall, however, that the presented analysis is only valid below the trough level while wave-induced mass flux is concentrated in the trough to crest region, and the below-trough contribution is minimal. One additional difference is the omission of the $\overline{\tilde{v}\tilde{w}}$ which is expected to be small due to the phasing difference in the vertical and horizontal directions and the small wave angle in the rotated coordinate system.

$$\bar{v} = \overline{v_\delta} + \frac{1}{\nu_t}\int_0^z \int_0^z G_y \, dz \, dz + \frac{\partial}{\partial x}\left\{ \frac{H_{rms}^2 \omega^2}{8k\nu_t} \frac{\sin\alpha}{\sinh^2 k\bar{h}} \left(\frac{\cosh 2kz'}{8k} + \frac{kz'^2}{4} - \frac{1}{8k} \right) \right\}$$

$$+ \frac{\tau_{by}}{\rho\nu_t} z' + \frac{g}{2\nu_t} \frac{\partial \bar{\eta}}{\partial y} z'^2 + \frac{\partial}{\partial y}\left\{ \frac{H_{rms}^2 \omega^2}{8k\nu_t} \frac{\sin^2\alpha}{\sinh^2 k\bar{h}} \left(\frac{\cosh 2kz'}{8k} + \frac{kz'^2}{4} - \frac{1}{8k} \right) \right\}$$

$$G_y = \frac{\partial \bar{v}}{\partial t} + \frac{\partial \bar{u}\,\bar{v}}{\partial x} + \frac{\partial \overline{v}^2}{\partial y} \approx \frac{\partial}{\partial t}\frac{Q_y}{\bar{h}} + \frac{\partial}{\partial x}\frac{Q_x Q_y}{\bar{h}^2} + \frac{\partial}{\partial y}\frac{Q_y^2}{\bar{h}^2} \tag{29}$$

Again, invoking the volume balance leads to an expression for the near-bottom velocity as follows:

$$\overline{v_\delta} = \frac{Q_y}{\bar{h}} - \frac{G_y d_t^2}{6\nu_t} - \frac{\partial}{\partial x}\left\{ \frac{H_{rms}^2 \omega^2}{8k\nu_t} \frac{\sin\alpha}{\sinh^2 k\bar{h}} \left(\frac{\sinh 2kd_t}{16k^2 d_t} + \frac{kd_t^2}{12} - \frac{1}{8k} \right) \right\}$$

$$- \frac{\tau_{by}}{2\rho\nu_t} d_t + \frac{g}{6\nu_t} \frac{\partial \bar{\eta}}{\partial y} d_t^2 - \frac{\partial}{\partial y}\left\{ \frac{H_{rms}^2 \omega^2}{8k\nu_t} \frac{\sin^2\alpha}{\sinh^2 k\bar{h}} \left(\frac{\sinh 2kd_t}{16k^2 d_t} + \frac{kd_t^2}{12} - \frac{1}{8k} \right) \right\} \tag{30}$$

where, as before, the depth-uniform version of G_y was used in the interest of brevity.

Finally, the longshore current profile within the boundary layer is expressed as follows:

$$\bar{v} = \frac{\bar{v}_\delta}{\ln \frac{30\delta}{k_n}} \ln \frac{30z}{k_n} \qquad \text{for} \qquad z < \delta \tag{31}$$

The depth-varying longshore currents prescribed by this stress-resolving method, Equation 29 along with Equation 30, are shown in Figure 15 as black lines, where the solid line accounts for the effect of the steady currents and the dashed line neglects the steady contribution. As in the case of cross-shore currents, the effect of the steady currents on the depth variation is unimportant and can be neglected.

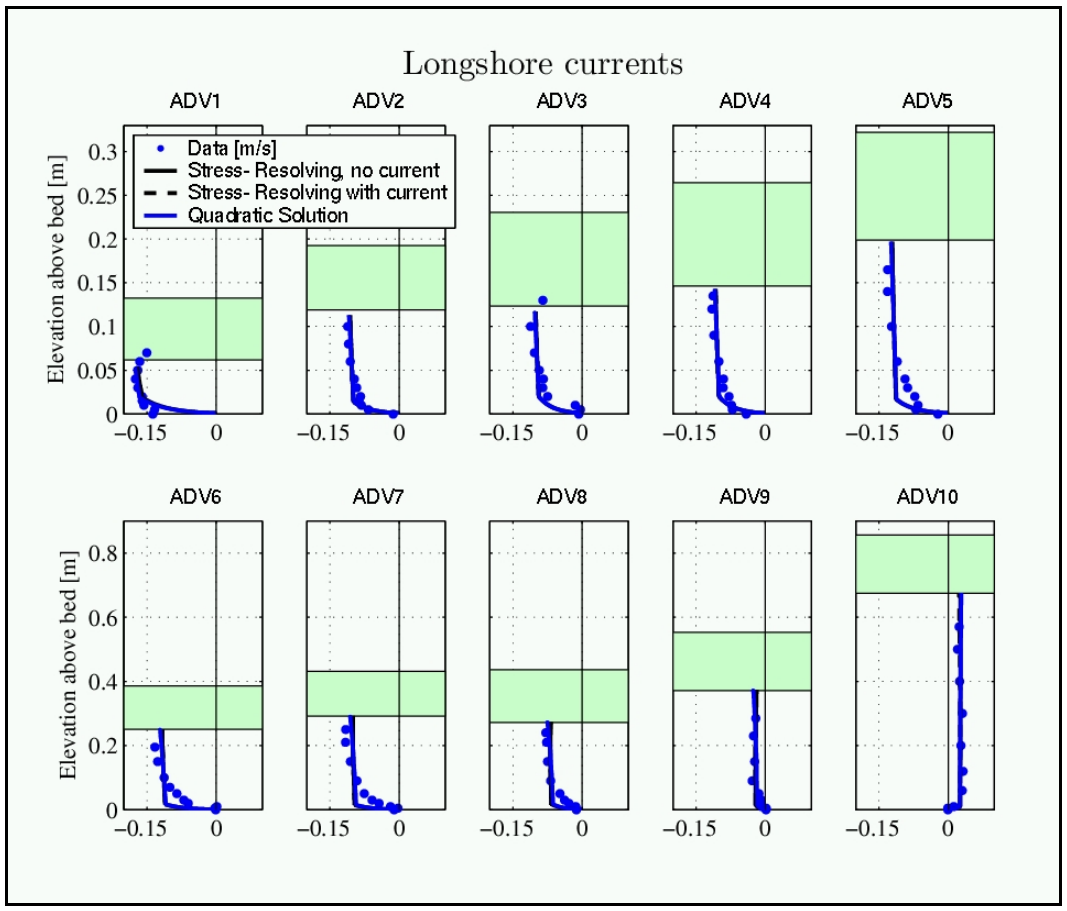

Figure 15. Depth-variation of longshore currents.

Simple alternative

As an alternative to the detailed approach outlined, a quadratic profile can be assumed a priori, which has precedent in several modeling efforts. Both Cox and Kobayashi (1997) and Garcez Faria et al. (2000) have used quadratic depth variation in modeling steady cross-shore flow, for instance. Also, the nearshore model SHORECIRC (Svendsen et al. 2002) assumes quadratic profiles for alongshore and cross-shore directed currents.

Adoption of a parabolic profile extending from outside of the boundary layer to the wave trough level is tantamount to assuming that eddy viscosities and organized wave forcing are depth independent. Several studies have indicated that the constant forcing distribution is justifiable based on laboratory experiments (Stive and Wind 1982, 1986). However, this simplification remains theoretically justifiable for long waves only.

Without a representation of the momentum contributions through the water column, a total of three boundary conditions or constraints must be

developed to uniquely determine the three coefficients. As previously done, it is assumed that the bottom shear stress is known and that the total volumetric flux can be developed. The third boundary condition can be derived from a shear stress applied at the wave trough level. As indicated by Dyhr-Nielsen and Sorenson (1970), a variation in wave height in the surf zone can develop a surface shear stress. The simple relation between wave height and surface shear stress τ_s is (Fredsoe and Deigaard 1992)

$$\tau_{sx} = \frac{-\rho g}{8}\frac{\partial H_{rms}^2}{\partial x}\cos^2\alpha + \tau_x^{wind} \qquad ; \qquad \tau_{sy} = \frac{-\rho g}{8}\frac{\partial H_{rms}^2}{\partial x}\cos\alpha\sin\alpha + \tau_y^{wind} \tag{32}$$

Expressing the velocity as a quadratic function in z and applying shear stress conditions on the bottom and at the surface and enforcing the local volume balance leads to

$$u = \frac{Q_x}{\bar{h}} - \frac{\sqrt{g\bar{h}}}{8}\left(\frac{H_{rms}}{\bar{h}}\right)^2\cos\alpha - \frac{d_t}{6\rho\nu_t}\left\{2\tau_{bx} + \tau_{sx}\right\} + \frac{\tau_{bx}}{\rho\nu_t}z' + \frac{1}{2\rho\nu_t d_t}\left\{\tau_{sx} - \tau_{bx}\right\}z'^2$$

$$v = \frac{Q_y}{\bar{h}} - \frac{d_t}{6\rho\nu_t}\left\{2\tau_{by} + \tau_{sy}\right\} + \frac{\tau_{bx}}{\rho\nu_t}z' + \frac{1}{2\rho\nu_t d_t}\left\{\tau_{sy} - \tau_{by}\right\}z'^2 \tag{33}$$

The simple alternative has some appeal in including the wind stress explicitly, although theoretically, a wind stress should be included implicitly in the stress-resolving technique previously outlined through an alteration bed shear stress.

The depth variation prescribed by Equation 33, labeled the Quadratic solution, is shown in Figures 14 and 15. Clearly, in both cases the differences in the depth-variation indicated by the simple alternative and the stress-resolving method are minimal.

Effect of depth variation on integrated solution

In using a 2-DH model, error is introduced when the depth-variation of the slowly-varying currents is neglected, and it is feasible to include the effect of this depth variation through a modification in the radiation stress. However, the significance of this omission continues to be a topic of considerable interest. Svendsen and Putrevu (1994) concluded that the dispersive effect due to vertical nonuniformities was an order of magnitude larger than the turbulent mixing. Conversely, Kobayashi et al. (1997) con-

cluded that the dispersion effects due to the local nonuniformities may play a significant role for monochromatic waves, but proved unimportant for irregular waves.

The laboratory data are used to determine, for cases of gradually varying coasts, the relative importance of the steady contribution when compared to the wave-induced contribution. Johnson and Smith (2005) apportioned the momentum fluxes into steady and wave momentum fluxes. The results are shown in Figure 16.

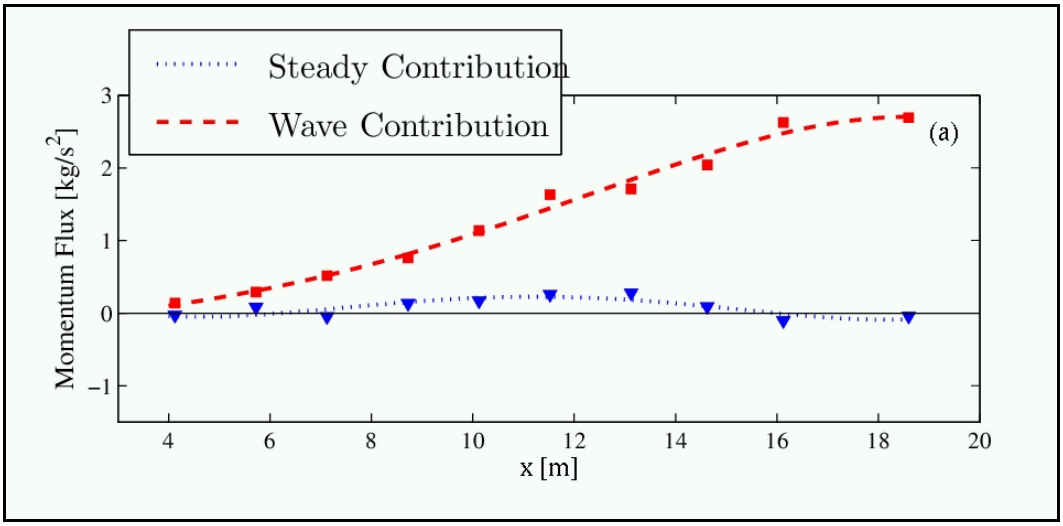

Figure 16. Current and wave contributions to the momentum flux.

Consistent with the previous statement that current interaction has little influence on the profile shape, it is clear in Figure 16 that the total momentum contribution is dominated by the wave motion. In essence for random waves, the effects of the depth-variation of the currents can justifiably be neglected in predicting U and V in the surf zone.

5 Conclusions

A detailed set of laboratory data are presented to demonstrate the significance of various terms in nearshore current prediction. The depth-dependent forms of radiation stress are presented along with an analysis showing that using a simple constant forcing over the depth is adequate to represent the inviscid (linear) wave forcing. Also, the recommendation is given to avoid basing depth-dependence of currents on the linear-wave stress distribution alone.

The bottom shear stress, as estimated from the residual in the alongshore momentum balance using LSTF data, functions as a standard to compare several stress models applied in the breaking region. The vertical dependence of the quadratic-based shear is found to be small considering the uncertainty in drag coefficients. Manning's formulations generally underpredicted stress, while the stress using wave friction factors were overpredicted by a factor of 2. The drag coefficient recommended in Thornton and Guza (1981) produced good results over the surf zone. Vertical profiles of currents in the inner surf zone demonstrate a departure from the G-M model, and shear stress was overpredicted. It is demonstrated that basing the bottom shear stress estimates on the steady currents alone results in gross error in the surf zone, while the square-wave approximation yields reasonable results.

Two methods of determining the distribution of currents over the water column are developed that depend on the 2-DH solution and the wave field. It is shown that the current-current interaction has little influence on the profile, and that it can justifiably be neglected. A simple solution that assumes that the currents are adequately described by a quadratic function yields results that are essentially equivalent to the more rigorous method.

References

Bouws, E., H. Gunther, W. Rosenthal, and C. L. Vincent. 1985. Similarity of the wind wave spectrum in finite depth water. 1. Spectral form. *J. Geophys. Res.* 90(C1): 975–986.

Cox, D. T., N. Kobayashi, and A. Okayasu. 1996. Bottom shear stress in the surf zone. *J. Geophys. Res.* 101(C6): 14337–14348.

Cox, D. T., and N. Kobayashi. 1997. A kinematic undertow model with a logarithmic boundary layer. *J. Wtrwy., Port, Coast. and Oc. Eng.* ASCE, 123(6): 354–360.

Cox, D. T., and N. Kobayashi, 2000. Identification of intense, intermittent coherent motions under shoaling and breaking waves. *J. Geophys. Res.* 105(C6): 14223–14236.

Dean, R. G., and R. A. Dalrymple. 1984. *Water wave mechanics for engineers and scientists.* Prentice-Hall, Englewood Cliffs, N.J.

Dyhr-Nielsen, M., and T. Sorensen. 1970. Some sand transport phenomena on coasts with bars. *Proc. of 12th Coast. Eng. Conference,* ASCE, 855–866.

Feddersen, F., R. T. Guza, S. Elgar, and T. H. C. Herbers. 1998. Longshore momentum balances in the nearshore. *J. Geophys. Res.* 103: 15667–15676.

Fredsoe, J., and R. Deigaard. 1992. *Mechanics of coastal sediment transport.* World Scientific, ISBN 9810208405, 369 p.

Garcez Faria, A. F., E. B. Thornton, T. C. Lippmann, and T. P. Stanton 2000. Undertow on a barred beach. *J. Geophys. Res.* 105(C7): 16999–17010.

Grant, W. D., and O. S. Madsen. 1979. Combined wave and current interaction with a rough bottom. *J. Geophys. Res.* 84(C4): 1797–1808.

Hamilton, D. G., and B. A. Ebersole. 2001. Establishing uniform longshore currents in a large-scale laboratory facility. *Coastal Eng.* 42: 199–218.

Hamilton, D. G., B. A. Ebersole, E. R. Smith, and P. Wang. 2001. Development of a large-scale laboratory facility for sediment transport research. ERDC/CHL TR-01-22. Vicksburg, MS: U.S. Army Engineer Research and Development Center.

Johnson, B. D., and J. M. Smith. 2005. Longshore current forcing by irregular waves. *J. Geophys. Res.*, 110, C06006, doi:10.1029/2004JC002336.

Karambas, T. V., and C. Koutitas. 2002. Surf and swash zone morphology evolution induced by nonlinear waves. *J. Wtrwy., Port, Coast. and Oc. Eng.* ASCE, 128(3): 102–113.

Kennedy, A. L., D. T. Cox, and N. Kobayashi. 1998. Application of an undertow model to irregular waves on barred beaches and reflective coastal structures. *Proc. of 26th Coast. Eng. Conference*, ASCE 311–324.

Kobayashi, N., and B. D. Johnson. 2001. Sand suspension, storage, advection and settling in surf and swash zones. *J. Geophysical Research* 106(C5): 9363–9376.

Kobayashi, N., E. A. Karjadi, and B. D. Johnson. 1997. Dispersion effects on longshore currents in surf zones. *J. Wtrwy., Port, Coast. and Oc. Eng.* ASCE, 123(5): 240–248.

Lesser, G. R., J. A. Roelvink, J. A. T. M. van Kester, and G. S. Stelling. 2004. Development and validation of a three-dimensional morphological model. *Coastal Eng.* 51: 883-915.

Lin, P., and P. L. Liu. 1998. Turbulence transport, vorticity dynamics, and solute mixing under plunging breaking waves in surf zone. *J. Geophys. Res.* 103(C8): 15677–15694.

Longuet-Higgins, M. S. 1970. Longshore currents generated by obliquely incident sea waves. Parts 1 and 2. *J. Geophys. Res.*, 756778–756801.

Madsen, O. S., and P. Salles. 1999. Eddy viscosity models for wave boundary layers. *Proc. 26th ICCE*, ASCE, 2615–2627.

Madsen, O. S. 1995. Spectral wave-current bottom boundary layer flows. *Proc. 24th ICCE*, ASCE, 384-398.

Nielsen, P. 1992. *Coastal bottom boundary layers and sediment transport.* River Edge, NJ: World Scientific.

Nishimura, H. 1982. Numerical simulation of nearshore circulation. *Proc. of 29th Japanese Conf. Coastal Eng.*, Japanese Society of Civil Engineers, 333–337 (in Japanese).

Reniers, A. J. H. M., and J. A. Battjes. 1997. A laboratory study of longshore currents over barred and non-barred beaches. *Coastal Eng.* 30, 1–21.

Rivero, F. J., and A. S. Arcilla. 1995. On the vertical distribution of $\langle \tilde{u}\tilde{w} \rangle$. *Coastal Eng.* 25: 137–152.

Ruessink, B. G., J. R. Miles, F. Feddersen, R. T. Guza, and S. Elgar. 2001. Modeling the alongshore current on barred beaches. *J. Geophys. Res.* 106: 22451–22463.

Smith, J. M., M. Larson, and N. C. Kraus.1993. Longshore current on a barred beach: Field measurements and calculations. *J. Geophys. Res.* 98(C12): 22717–22731.

Smith, J. M., A. R. Sherlock, and D. T. Resio. 2001. STWAVE: Steady-state spectral wave model user's guide for STWAVE Version 3. ERDC/CHL SR-01-01. Vicksburg, MS: US Army Engineer Research and Development Center.

Stive, M. J. 1980. Velocity and pressure field of spilling breakers. *Proc., 17th Coast. Engrg. Conf.* ASCE, 547–566.

Stive, M. J. F., and H. G. Wind.1982. A study of radiation stress and set-up in the nearshore region. *Coastal Eng.* 6: 1–25.

Stive, M. J. F., and H. G. Wind. 1986. Cross-shore mean flow in the surf zone. *Coastal Eng.* 10: 325–340.

Soulsby, R. L. 1997. *Dynamics of marine sands.* Thomas Teleford, London, UK.

Svendsen, I. A., and U. Putrevu. 1994. Nearshore mixing and dispersion. *Proc. Roy. Soc. Lond.* A(445): 561–576.

Svendsen, I. A., H. A. Schaffer and J. B. Hansen. 1987. The interaction between the undertow and the boundary layer flow on a beach. *J. Geophys. Res.* 92: 11,845-11,856.

Svendsen, I.A., K. Haas, and Q. Zhao. 2002. Quasi-3D nearshore circulation model SHORECIRC - Version 2.0," *Report CACR-02-01.* Newark, DE: Center for Applied Coastal Research, University of Delaware.

Swart, D. H. 1974. *Offshore sediment transport and equilibrium beach profiles.* Publication No. 131. The Netherlands: Delft Hydraulics Laboratory.

Tajima, Y. 2004. Waves, currents, and sediment transport in the surf zone along long, straight beaches. Ph.D. diss., Massachusetts Institute of Technology.

Thornton, E. B., and R. T. Guza. 1981. Longshore currents and bed shear stress. *Proc. Directional Wave Spectral Applications*, ASCE, 147–164.

Thornton, E. B., and R. T. Guza. 1986. Surf zone longshore currents and random waves: Field data and models. *J. Phys. Oceanogr.* 16: 1165–1178.

Trowbridge, J., and S. Elgar. 2001. Measurements of surf zone turbulence. *J. Phys. Oceanogr.* 31: 2403–2417.

Wang, P., B. A. Ebersole, E. R. Smith, and B. D. Johnson. 2002. Temporal and spatial variations of surf-zone currents and suspended sediment concentration. *Coastal Eng.* 46: 175–211.

Wikramanayake, P. N., and O. S. Madsen. 1994. Calculation of suspended sediment transport by combined wave-current flows. Technical Report DRP-94-7. Vicksburg, MS: U.S. Army Engineer Waterways Experiment Station.

Xia, H., Z. Xia, and L. Zhu.2004. Vertical variation in radiation stress and wave-induced current. *Coastal Eng.* 51: 309–321.

REPORT DOCUMENTATION PAGE

Form Approved
OMB No. 0704-0188

1. REPORT DATE *(DD-MM-YYYY)*	**2. REPORT TYPE**	**3. DATES COVERED** *(From - To)*
August 2006	Final Report	

4. TITLE AND SUBTITLE

Including Nearshore Processes in Phase-Averaged Hydrodynamic Models

5a. CONTRACT NUMBER

5b. GRANT NUMBER

5c. PROGRAM ELEMENT NUMBER

6. AUTHOR(S)

Bradley D Johnson

5d. PROJECT NUMBER

5e. TASK NUMBER

5f. WORK UNIT NUMBER

7. PERFORMING ORGANIZATION NAME(S) AND ADDRESS(ES)

Coastal and Hydraulics Laboratory
U.S. Army Engineer Research and Development Center
3909 Halls Ferry Road
Vicksburg, MS 39180-6199

8. PERFORMING ORGANIZATION REPORT NUMBER

ERDC/CHL TR-06-12

9. SPONSORING / MONITORING AGENCY NAME(S) AND ADDRESS(ES)

U.S. Army Corps of Engineers
Washington, DC 20314-1000

10. SPONSOR/MONITOR'S ACRONYM(S)

11. SPONSOR/MONITOR'S REPORT NUMBER(S)

12. DISTRIBUTION / AVAILABILITY STATEMENT

Approved for public release; distribution is unlimited.

13. SUPPLEMENTARY NOTES

14. ABSTRACT

The large spatial and time scales of the numerical modeling projects of the U.S. Army Corps of Engineers (USACE) requires the use of computationally efficient phase-averaged hydrodynamic models derived by averaging the equations of motion over a representative short wave period. Guidance in modeling nearshore regions with phase-averaged hydrodynamic models is provided herein. Physical processes unique to the surf zone are described along with methods of incorporating these effects to improve hydrodynamic predictions. Comparisons to detailed measurements from a laboratory basin experiment are used to demonstrate the significance of including processes unique to nearshore regions. To provide guidance that is applicable to varied phase-averaged models, details of the implementation are not provided herein, and the focus is on conceptual models

15. SUBJECT TERMS

Nearshore
Radiation stress
Breaking waves
Bottom shear stress
Shear stress
Roller

16. SECURITY CLASSIFICATION OF:			**17. LIMITATION OF ABSTRACT**	**18. NUMBER OF PAGES**	**19a. NAME OF RESPONSIBLE PERSON**
a. REPORT	**b. ABSTRACT**	**c. THIS PAGE**			**19b. TELEPHONE NUMBER** *(include area code)*
UNCLASSIFIED	UNCLASSIFIED	UNCLASSIFIED		48	